



# The solubility of apatite in H<sub>2</sub>O, KCl-H<sub>2</sub>O, NaCl-H<sub>2</sub>O at 800 °C and 1.0 GPa: Implications for REE mobility in high-grade saline brines



Philipp Mair<sup>a,\*</sup>, Peter Tropper<sup>a</sup>, Daniel E. Harlov<sup>b,c</sup>, Craig E. Manning<sup>d</sup>

<sup>a</sup> Institute of Mineralogy and Petrography, Faculty of Geo- and Atmospheric Sciences, University of Innsbruck, Innrain 52f, A-6020 Innsbruck, Austria

<sup>b</sup> Helmholtz Zentrum Potsdam, Deutsches GeoForschungsZentrum, Telegrafenberg, D-14473 Potsdam, Germany

<sup>c</sup> Department of Geology, University of Johannesburg, P.O. Box 524, Auckland Park 2006, South Africa

<sup>d</sup> Department of Earth and Space Sciences, University of California, Los Angeles, CA 90095-1567, USA

## ARTICLE INFO

Editor: K. Mezger

### Keywords:

Apatite solubility  
Experimental petrology  
REE mobility  
Metamorphic fluids  
pH model

## ABSTRACT

Apatite is an important host for LREE, F, and Cl and thus can be used to monitor elemental mass transfer in high P-T settings. In this investigation, the solubilities of synthetic fluor- and chlorapatite and natural Durango fluorapatite were measured in H<sub>2</sub>O, KCl-H<sub>2</sub>O, and NaCl-H<sub>2</sub>O fluids at 800 °C and 1.0 GPa, using the piston-cylinder apparatus. The solubility of apatite is reported in parts/million by weight (ppm), and is calculated via the formula  $m_{Ap} = [(\Delta m_{Ap} / H_2O + KCl \text{ or } NaCl + \Delta m_{Ap}) * 10^6]$ , where  $\Delta m_{Ap} = m_{Ap-in} - m_{Ap-out}$ . The experimental results indicate a strong increase in apatite solubility in aqueous fluids with moderate KCl and NaCl mole fractions ( $X_{KCl}$  and  $X_{NaCl}$ ). Under all conditions, synthetic fluorapatite and synthetic chlorapatite dissolve congruently. The solubility of synthetic fluorapatite increases from 19 ppm in pure H<sub>2</sub>O to 2123 ppm at  $X_{KCl} = 0.52$ . The solubility of synthetic chlorapatite rises from 37 ppm in pure H<sub>2</sub>O to 2590 ppm at  $X_{KCl} = 0.50$ . At  $X_{KCl} > 0.5$  the solubility of synthetic fluorapatite decreases to 1691 ( $X_{KCl} = 0.72$ ) and the solubility of synthetic chlorapatite decreases to 2284 ppm ( $X_{KCl} = 0.65$ ). In contrast, natural Durango fluorapatite dissolves incongruently at  $X_{KCl} < 0.2$  to monazite + fluid and congruently at  $X_{KCl} > 0.2$ . The solubility of natural Durango fluorapatite increases from 70 ppm in pure H<sub>2</sub>O to 2073 ppm at  $X_{KCl} = 0.50$  respectively. In contrast to the KCl-H<sub>2</sub>O system, apatite solubilities are considerably higher in the NaCl-H<sub>2</sub>O system. The solubility of synthetic fluorapatite increases to 4909 ppm at  $X_{NaCl} = 0.51$  and the solubility of synthetic chlorapatite rises to 5144 ppm at  $X_{NaCl} = 0.50$ . Compared to fluorite, calcite and anhydrite, apatite solubility is significantly lower in H<sub>2</sub>O, NaCl-H<sub>2</sub>O, and KCl-H<sub>2</sub>O. After completion of each experiment, the pH was measured and a comprehensive step-by-step procedure (limiting reactant concept) was used to model the observed quench pH in the system apatite-KCl-H<sub>2</sub>O.

## 1. Introduction

Aqueous fluids are increasingly recognized as playing an important role in elemental transport in high P-T environments. Understanding the scale and magnitude of fluid-mediated compositional change associated with saline brines is central to the understanding of geochemical processes in deep crustal/upper mantle environments (e.g., Newton and Manning, 2010; Harlov et al., 2016). The origins of these saline, multicomponent fluids are still debated (e.g., Banks et al., 2000; Touret, 2001; Yardley and Graham, 2002), but experimental evidence suggests that regardless of their origin they are important agents of rock alteration and mass transfer wherever they occur (e.g., Newton et al., 1998; Newton and Manning, 2010; Rapp et al., 2010; Aranovich et al., 2013).

The generation and migration of alkali-halide brines play an important role in mass transport (e.g. K-metasomatism) and mineral-fluid-melt phase equilibria in the lower crust and upper mantle (e.g., Newton et al., 1998; Touret, 2001; Yardley and Graham, 2002; Harlov and Förster, 2002; Harlov et al., 2006; Hansen and Harlov, 2007, 2009; Newton and Manning, 2010; Rapp et al., 2010; Glassley et al., 2010; Aranovich et al., 2013, 2014; Manning and Aranovich, 2014). Fluid inclusions containing chloride brines with > 10 wt% NaCl equivalent have been reported from granulites (e.g., Touret, 2001), eclogites (e.g., Philippot and Selverstone, 1991), and mantle diamonds (e.g., Izraeli et al., 2001). In addition, crystalline salts have been observed in high-grade metamorphic rocks (Markl et al., 1998). Calcium-rich silicates record equilibration of minerals with saline fluids in a range of metamorphic settings (e.g., Nijland et al., 1993; Markl and Piazzolo, 1998;

\* Corresponding author.

E-mail address: [philipp.mair@uibk.ac.at](mailto:philipp.mair@uibk.ac.at) (P. Mair).

Markl et al., 1998). Finally, magnetotelluric observations suggest the presence of conductive, saline solutions in deep-crustal fault zones (e.g., Wannamaker et al., 2004). Field studies of high-grade metamorphic rocks show that mobility of REE and Y in granulite-facies terranes is greatly enhanced in the presence of high-grade fluids (e.g., Pan and Fleet, 1996; Markl et al., 1998; Newton et al., 1998; Touret, 2001; Harlov et al., 2006; Hansen and Harlov, 2007, 2009; Glassley et al., 2010). REE (and by extension, Y) mobility can be enhanced by dissolved halogens in some cases as highly concentrated solutions (Pan and Fleet, 1996; Schmidt et al., 2007; Antignano and Manning, 2008; Pournier et al., 2010; Newton and Manning, 2010).

Potassium species are important constituents of high-grade metamorphic fluids (e.g., Aranovich and Newton, 1997; Newton et al., 1998; Harlov and Förster, 2002). Potassium metasomatism has also been recognized by field workers in high-grade metamorphic terranes (e.g., Harlov and Förster, 2002; Glassley et al., 2010). Concentrated salt solutions seem, because of their high mechanical mobility and alkali-exchanging potential, feasible as metasomatic fluids for a variety of deep crust and upper mantle processes. Aranovich and Newton (1997) found that the KCl component in a brine lowers the H<sub>2</sub>O activity even more than does NaCl at a given *T*, *P*, and *X*<sub>H<sub>2</sub>O</sub>, and that the KCl activity is lower for a given salt concentration than the NaCl activity (Aranovich and Newton, 1996). For the H<sub>2</sub>O–KCl system only very few relevant experimental data exist. Anderson and Burnham (1967) and Shmulovich et al. (2006) conducted quartz solubility measurements in H<sub>2</sub>O–KCl. Aranovich and Newton (1997) determined the *α*-*X* relations of fluids in this system.

Apatite (Ca<sub>5</sub>(PO<sub>4</sub>)<sub>3</sub>(OH,F,Cl)) is a ubiquitous accessory mineral in most crustal rocks. With respect to its occurrence, chemical diversity, high affinity for many trace metals (e.g., REE) and major repository of halogens (F, Cl), the presence of apatite can be used for “fingerprinting” metasomatic processes and to monitor elemental mass transfer in high P–*T* settings. (e.g., Spear and Pyle, 2002; Harlov, 2015; Hughes and Rakovan, 2015; Kusebauch et al., 2015a, 2015b). The presence of F and Cl in crustal and mantle fluids is economically important because of their role in REE ore deposit formation (e.g., Andreoli et al., 1994; Fayek and Kyser, 1997; Salvi et al., 2000; Chakhmouradian and Wall, 2012; Williams-Jones et al., 2012) as well as their contribution in tracing magmatic (e.g., Pollard et al., 1987; Webster et al., 1999; Markl et al., 1998; Agangi et al., 2010) and metamorphic (e.g., Yardley, 1985; Brenan, 1993) processes. An important first step in using apatite as a monitor of elemental mass transfer is the determination of its solubility (in ppm) in aqueous fluids of various compositions at high *P* and *T* (e.g., Antignano and Manning, 2008). It is therefore essential to understand the solubility of apatite behaviour with respect to P–*T*–*X*<sub>i</sub> conditions and polymerization during the metasomatic processes that attend lower crustal and upper mantle high-grade metamorphism.

Previous experimental results of apatite solubility at high P–*T* conditions, done by Ayers and Watson (1991) and Antignano and Manning (2008) using natural Durango fluorapatite, yielded strongly contrasting and hence problematic results. Ayers and Watson (1991) reported relatively high apatite solubilities ranging from 500 ppm to 4400 ppm in pure H<sub>2</sub>O at 800–1200 °C and 1.0–3.0 GPa which increased with rising temperature. They also reported decreasing solubility with increasing pressure and observed no change with the addition of NaCl. This behaviour is in strong contrast with that of other Ca compounds such as calcite (CaCO<sub>3</sub>), fluorite (CaF<sub>2</sub>), and anhydrite (CaSO<sub>4</sub>), for which the calcium cation (Ca<sup>2+</sup>) is the controlling factor, as well as pressure and elevated NaCl concentrations which promote greater solubility (Caciagli and Manning, 2003; Tropper and Manning, 2007a; Newton and Manning, 2005; Newton and Manning, 2010). In an effort to identify the cause of apparent differences in apatite solubility behaviour relative to that of similar minerals, and to extend solubility measurements to aid the study of deep fluid–rock interaction, Antignano and Manning (2008) undertook a systematic investigation of the solubility of the Durango fluorapatite in pure H<sub>2</sub>O and NaCl–H<sub>2</sub>O at 700–900 °C

and 0.7–2.0 GPa. The amount of dissolved fluorapatite ranging from 56 ppm to 288 ppm in pure H<sub>2</sub>O was low at all investigated P–*T* conditions, but increased with increasing *T* and *P*. Their results from the apatite dissolution experiments in the NaCl–H<sub>2</sub>O system demonstrated a strong increase in dissolved fluorapatite concentrations with rising NaCl mole fraction (*X*<sub>NaCl</sub>) at all *P* and *T*, and *X*<sub>NaCl</sub> to near halite saturation. Expanding on the Durango fluorapatite–H<sub>2</sub>O and Durango fluorapatite–NaCl–H<sub>2</sub>O experiments of Ayers and Watson (1991) and Antignano and Manning (2008) in this study, we present new apatite solubility data at 800 °C and 1.0 GPa via a series of new solubility measurements involving synthetic fluorapatite, synthetic chlorapatite, and the Durango fluorapatite in aqueous fluids in the system H<sub>2</sub>O, KCl–H<sub>2</sub>O, and NaCl–H<sub>2</sub>O at 800 °C and 1.0 GPa.

## 2. Experimental methods

Experiments were conducted on synthetic crystals of fluorapatite (Ca<sub>5</sub>(PO<sub>4</sub>)<sub>3</sub>F) and chlorapatite (Ca<sub>5</sub>(PO<sub>4</sub>)<sub>3</sub>Cl), and inclusion-free, gem-quality fluorapatite from Durango, Mexico, which contains ~3.5 wt% F and ~1–2 wt% LREE, respectively (Young et al., 1969; Antignano and Manning, 2008). The synthetic fluorapatite and chlorapatite were synthesized using the flux technique described in Schettler et al. (2011). The flux consisted of 0.1 mol of CaF<sub>2</sub> (7.808 g) or CaCl<sub>2</sub> (11.098 g) thoroughly dry mixed with 0.03 mol of Ca<sub>3</sub>(PO<sub>4</sub>)<sub>2</sub> (9.305 g). The dry mix was packed into 30 ml volume Pt crucible and pressed down using the pestle. The Pt crucible, with a loose fitting Pt cover, was then placed in a programmable high temperature oven and the temperature ramped up to 1375 °C over a period of 4 h. The melt was allowed to equilibrate or ‘soak’ at 1375 °C for 15 h and then slowly cooled to 1220 °C at a rate of 3 °C/h during which time either fluorapatite or chlorapatite crystals nucleated in the melt and grew in size. After anywhere from 1 to 20 h at 1220 °C, the crucible was removed from the oven and quenched in air for a period of about 30 min until it was cool enough to extract the flux-crystal mass as a solid lump. The apatite crystals were separated from the flux by boiling the quenched flux + crystals in distilled water in a 2 l beaker. If the flux consisted of CaF<sub>2</sub>, the flux + crystals were boiled in an aqueous 20% solution of Al(NO<sub>3</sub>)<sub>3</sub>·9H<sub>2</sub>O in order to dissolve out the residual CaF<sub>2</sub>. The resulting transparent, light blue-green, euhedral to semi-euhedral fluor- and chlorapatite crystals range from 100 μm up to 6–7 mm in length and from 20 μm to 3–4 mm in diameter. The smaller crystals are inclusion-free whereas the majority of the larger crystals (> 1 mm) tend to contain a few scattered melt inclusions.

Single crystals, optically free of flux melt inclusions, were selected for use in the solubility studies. The crystals were first ground into ~2–3 mm long ellipsoids using 400-grit emery paper to remove sharp edges, and then rolled in 800-grit emery paper until they acquired a polish. The polished crystals were cleaned in ethanol in an ultrasonic bath, and then dried at 120 °C for 15 min. This procedure generated single crystals that ranged in weight from 1 to 3 mg (Tables 1a, 1b). Each experiment consisted of an outer Pt capsule (outer diameter: 3.0 mm, thickness: 0.2 mm) and an inner Pt capsule (outer diameter: 2.0 mm, thickness: 0.1 mm) in which the apatite single crystal was placed. Thick-walled Pt (0.2 mm) was used for the outer capsule to prevent puncture. The use of an inner capsule protected the crystal and minimized the thermal gradient in the capsule assembly (Tropper and Manning, 2005). To facilitate H<sub>2</sub>O penetration while ensuring crystal containment during the experiments, the inner Pt capsule was lightly crimped and closed with a pair of pliers. The inner Pt capsule, plus precisely weighed quantities of KCl, NaCl and H<sub>2</sub>O (Tables 1a, 1b), were then placed in the outer Pt capsule. The outer Pt capsule was sealed by arc-welding and then placed in a 120 °C oven for 30 min to check for leakage.

All experiments were performed at 800 °C and 1000 MPa in a non-end-loaded piston-cylinder apparatus, using 22 mm diameter NaCl assemblies with a cylindrical graphite oven and sealed by pyrophyllite rings. Each double capsule assembly was placed horizontally at the

**Table 1a**  
Experimental results in the system Apatite-H<sub>2</sub>O-KCl at 800 °C and 1.0 GPa.

Run number	Time (h)	H <sub>2</sub> O in (mg)	KCl in (mg)	X <sub>KCl</sub>	Apatite in (mg)	Apatite out (mg)	Solubility (ppm)	pH
Durango-Apatite - H <sub>2</sub> O - KCl								
Durango-Ap_006	24	40,06	0,00	0,00	1,3163	1,3135	70 (6)	6,5
Durango-Ap_015	24	35,20	16,58	0,10	2,6259	2,5676	1124 (11)	7,5
Durango-Ap_017	24	25,81	26,19	0,20	1,4445	1,3596	1630 (4)	7,5
Durango-Ap_018	24	17,19	31,60	0,31	0,8417	0,7571	1732 (6)	7,5
Durango-Ap_020	24	14,26	39,06	0,40	0,5335	0,4268	1998 (2)	7,5
Durango-Ap_010	24	9,16	37,19	0,50	0,6143	0,5180	2073 (6)	7,0
Durango-Ap_011	24	5,93	45,97	0,65	0,8453	0,7587	1665 (5)	6,5
Synthetic F-Apatite - H <sub>2</sub> O - KCl								
F-Ap_005	24	39,60	0,00	0,00	1,3137	1,3129	19 (3)	6,5
F-Ap_009	24	36,00	16,49	0,10	0,8642	0,8007	1210 (6)	7,5
F-Ap_012	24	26,86	27,18	0,20	0,5704	0,4880	1521 (10)	7,5
F-Ap_013	24	19,72	34,07	0,30	1,5636	1,4710	1719 (12)	7,5
F-Ap_014	24	13,75	38,91	0,41	0,3893	0,2881	1917 (6)	7,5
F-Ap_007	24	8,36	37,49	0,52	0,8939	0,7964	2123 (6)	6,5
F-Ap_008	24	4,82	51,79	0,72	0,8949	0,7990	1691 (7)	6,0
Synthetic Cl-Apatite - H <sub>2</sub> O - KCl								
Cl-Ap_007	24	40,13	0,00	0,00	0,5355	0,5340	37 (6)	7,5
Cl-Ap_021	24	34,82	17,11	0,11	0,6822	0,6045	1495 (6)	7,5
Cl-Ap_023	24	26,35	27,06	0,20	0,5997	0,5024	1819 (3)	6,5
Cl-Ap_024	24	18,14	33,79	0,31	0,9169	0,7993	2260 (8)	5,0
Cl-Ap_025	24	14,05	38,99	0,40	0,3905	0,2583	2487 (4)	5,0
Cl-Ap_009	24	9,08	38,08	0,50	0,5884	0,4659	2590 (20)	3,5
Cl-Ap_010	24	5,91	45,60	0,65	0,4934	0,3755	2284 (6)	4,0

center of the NaCl assembly surrounded by the graphite-furnace and packed in NaCl. It was covered with a small, thin pyrophyllite sheet to prevent puncture by the thermocouple. Pressure and temperature was monitored using a pressure gauge and a NiCr-Ni thermocouple, respectively. Pressure was maintained to within 200 bar gauge pressure and the accuracy of the reported temperature is estimated to be  $\pm 2$  °C. Experiments were initially brought to 0.2 GPa and 100 °C and held for 15 min. An experiment was then heated and pressed to 800 °C and 1.0 GPa following a temperature and pressure ramp of 20 °C/min and 0.02 GPa/min. After 24 h the experiments were quenched to  $T < 150$  °C within several seconds by shutting off the power to the graphite oven. After each experiment, the outer capsule was pierced with a needle, and the pH of the quench fluid was checked with a pH testing paper (Tables 1a, 1b). After drying for 30 min at 120 °C, the apatite crystal was then extracted from the inner capsule, treated ultrasonically in ethanol to remove adhering quench precipitate, dried at 120 °C, and weighed with a Mettler Toledo XP2U ultra-microbalance ( $1\sigma = 0.1 \mu\text{g}$ ) (Tables 1a, 1b). All apatite grains were then examined

optically with a binocular microscope, in which single crystals from selected experiments were mounted onto double-sided carbon tape and characterized by scanning electron microscope (SEM) (Fig. 1).

The solubility of the apatite is reported in parts/million by weight (ppm), and is calculated  $m_{\text{Ap}} = [(\Delta m_{\text{Ap}} / \text{H}_2\text{O} + \text{KCl or NaCl} + \Delta m_{\text{Ap}}) * 10^6]$ , where  $\Delta m_{\text{Ap}} = m_{\text{Ap-in}} - m_{\text{Ap-out}}$ . Monazite crystals were produced by incongruent dissolution of the starting Durango fluorapatite in the NaCl experiment (Fig. 1b, c), but their total weight was below the detection limit and hence ignored. Reported mole fractions of KCl and NaCl ( $X_{\text{KCl}}$  and  $X_{\text{NaCl}}$ ) were calculated from the starting ratio  $n_{\text{KCl}}/(n_{\text{KCl}} + n_{\text{H}_2\text{O}})$  and  $n_{\text{NaCl}}/(n_{\text{NaCl}} + n_{\text{H}_2\text{O}})$  in the experiment. KCl, NaCl, and H<sub>2</sub>O masses were determined on a Mettler Toledo AX205 DeltaRange microbalance ( $1\sigma = 0.03 \text{ mg}$ ) (Tables 1a, 1b). The composition of newly formed, secondary apatite was semi-quantitatively analyzed using a JEOL JSM-6010LV scanning electron microscope (SEM) equipped with a Quantax EDS (Bruker). For further speciation calculations the apatite mass loss ( $\Delta m_{\text{Ap}}$ ) and the measured pH were used to calculate ionic species by means of the concept of the

**Table 1b**  
Experimental results in the system Apatite-H<sub>2</sub>O-NaCl at 800 °C and 1.0 GPa.

Run number	Time (h)	H <sub>2</sub> O in (mg)	NaCl in (mg)	X <sub>NaCl</sub>	Apatite in (mg)	Apatite out (mg)	Solubility (ppm)	pH
Durango-Apatite - H <sub>2</sub> O - NaCl								
Durango-Ap_019	24	31.64	14.08	0.12	1.1618	1.0709	1985 (7)	8.0
Durango-Ap_020	24	28.37	22.81	0.20	1.6804	1.5366	2802 (5)	7.0
Durango-Ap_018	24	23.96	28.09	0.27	0.7307	0.5546	3372 (5)	7.5
Durango-Ap_021	24	17.20	36.84	0.40	1.7999	1.5742	4161 (6)	4.0
Durango-Ap_022	24	12.10	38.93	0.50	1.0628	0.8390	4367 (8)	4.5
Synthetic F-Apatite - H <sub>2</sub> O - NaCl								
F-Ap_037	24	37.54	14.13	0.10	1.0266	0.9170	2115 (3)	6.5
F-Ap_038	24	28.44	24.03	0.21	1.1134	0.9305	3473 (5)	3.5
F-Ap_039	24	21.76	31.13	0.31	0.6140	0.3910	4198 (5)	3.5
F-Ap_040	24	16.73	37.07	0.41	0.5693	0.3210	4594 (3)	3.5
F-Ap_041	24	11.60	39.08	0.51	0.8392	0.5892	4909 (6)	3.0
Synthetic Cl-Apatite - H <sub>2</sub> O - NaCl								
Cl-Ap_026	24	37.20	13.69	0.10	0.8950	0.7847	2162 (13)	5.5
Cl-Ap_027	24	28.48	23.93	0.21	0.5765	0.3726	3875 (6)	5.5
Cl-Ap_028	24	20.81	30.06	0.31	0.6557	0.4236	4541 (1)	5.5
Cl-Ap_033	24	15.18	32.43	0.40	0.5083	0.2808	4756 (3)	3.5
Cl-Ap_044	24	12.15	39.22	0.50	0.7170	0.4514	5144 (8)	3.5

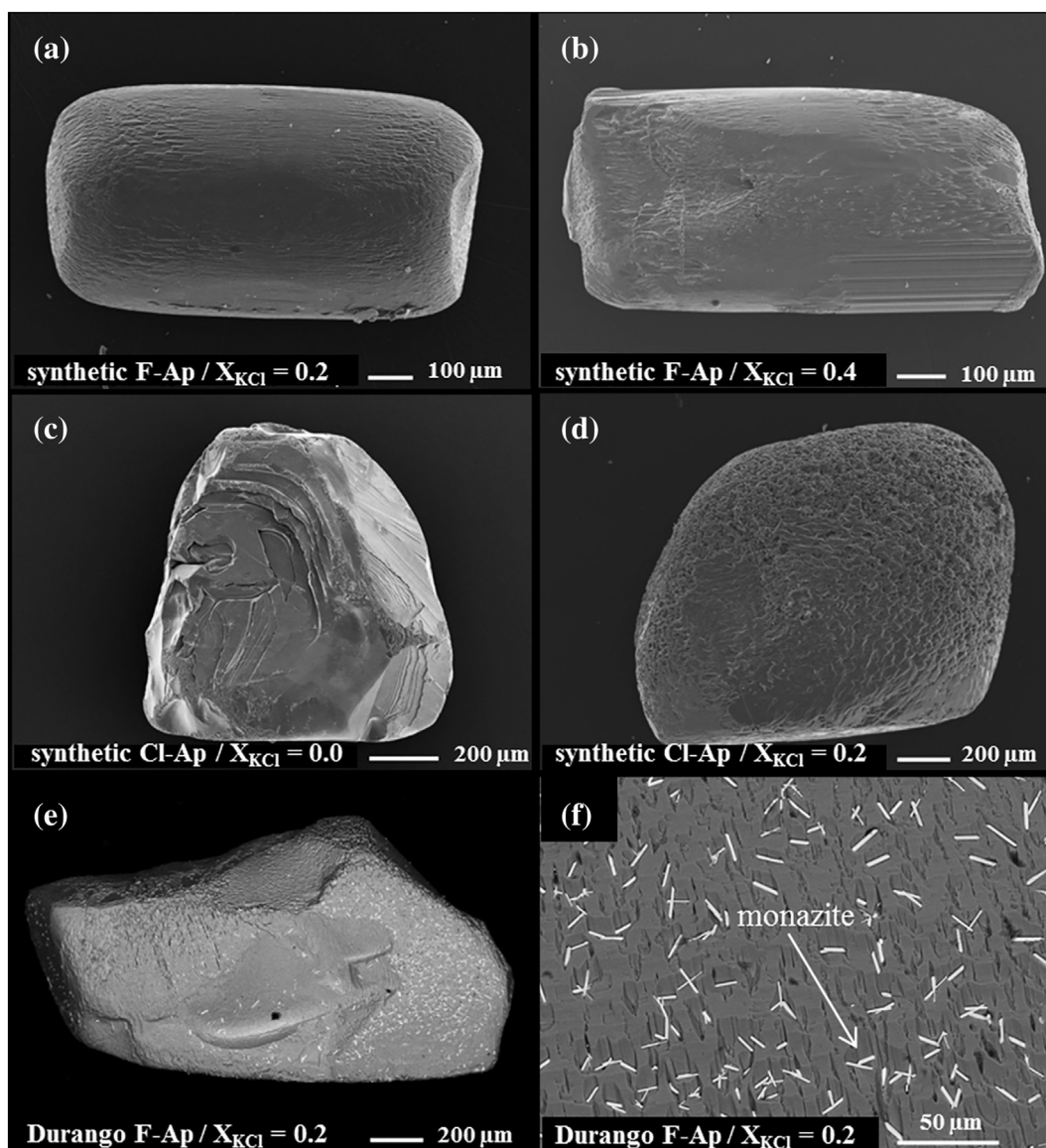


Fig. 1. SEM images of run products from selected experiments. (a, b, c, d) Residual apatite crystal illustrating solution-rounded edges, dissolution grooves and etch pits. (e, f) Micron-scale monazite crystals on the surface of incongruently dissolved starting Durango F-apatite.

limiting reactant (Tables 2a, 2b). The concept of the limiting reactant in the dissolution reaction of apatite refers to the substance that is totally consumed after completion of the chemical reaction. Hence the amount of products that can be formed is limited by the amount of this reactant ( $\Delta m_{Ap}$ ) (e.g., Petrucci et al., 2006; Mortimer et al., 2015).

### 3. Results

#### 3.1. Textures and equilibrium

The experimental results are given in Tables 1a and 1b. Run products included partly dissolved starting apatite crystals (Fig. 1), newly formed secondary apatite crystals in the outer capsules of some experiments (Fig. 2), monazite grains on the surfaces of apatite starting crystals (Fig. 1e, f) and sub-micron sized white powder of KCl (Fig. 2) or NaCl. The residual apatite crystals displayed solution-rounded edges and, in some cases, significant dissolution grooves, and etch pits (Fig. 1). The newly formed euhedral secondary apatite crystals occur as hollow, prismatic, hexagonal needles (Fig. 2), which were distributed randomly throughout the inner and outer capsules. The amount of secondary apatite needles increased with increasing  $X_{KCl}$  and  $X_{NaCl}$ ,

accompanied by an increase in apatite solubility (Tables 1a, 1b). The size of these apatite crystals was up to  $\sim 20\text{--}50\ \mu\text{m}$  along the c-axis and ranged from sparse and separate crystallites to fibrous aggregates which were mostly embedded in KCl or NaCl aggregates (Fig. 2). SEM analysis indicated that the Cl contents of the secondary apatites in the system  $\text{H}_2\text{O-KCl}$  rise successively with increasing  $X_{KCl}$  from  $X_{Cl(\text{in F-ap})} = 0.068 \pm 0.03$  ( $X_{KCl} = 0.20$ ) and  $X_{Cl(\text{in Cl-ap})} = 0.210 \pm 0.04$  ( $X_{KCl} = 0.20$ ) to  $X_{Cl(\text{in F-ap})} = 0.253 \pm 0.06$  ( $X_{KCl} = 0.72$ ) and  $X_{Cl(\text{in Cl-ap})} = 0.621 \pm 0.11$  ( $X_{KCl} = 0.65$ ) (Fig. 3a, b). Two generations of secondary apatite crystals with different size, morphology (Fig. 2d) and chemical composition (Fig. 3b) were found in the system chlorapatite- $\text{H}_2\text{O-KCl}$  at a mole fraction of  $X_{KCl} = 0.4$ . The first generation of quench apatites (sec ap I) can be recognized by its characteristic prismatic crystals (Fig. 2c, d). The second generation of apatites (sec ap II) occurs as stellate clusters of thin needles, which are significantly smaller than the apatite crystals of the first generation (Fig. 2d). The Cl content of the second apatite generation is  $X_{Cl(\text{in Cl-ap})} = 0.611 \pm 0.12$  and thus higher than the Cl content of the first generation of apatites ( $X_{Cl(\text{in Cl-ap})} = 0.345 \pm 0.07$ ) (Fig. 3b; Table 2b). Due to their morphology, high nucleation density, and abundance, we interpret these secondary apatite crystals, together with the KCl and NaCl aggregates, to represent

**Table 2a**  
Quench pH model of the system: F-apatite-H<sub>2</sub>O-KCl.

Reactants			Products						
F-apatite - H <sub>2</sub> O									
2 Ca <sub>5</sub> (PO <sub>4</sub> ) <sub>3</sub> F + 0.016 H <sub>2</sub> O			2 Ca <sub>5</sub> (PO <sub>4</sub> ) <sub>3</sub> (OH <sub>1-x</sub> , F <sub>x</sub> ) + (0.016-2(1-x)) OH <sup>-</sup> + 2(1-x) F <sup>-</sup> + 0.016H <sup>+</sup>						
			2 Ca <sub>5</sub> (PO <sub>4</sub> ) <sub>3</sub> (OH <sub>0.008</sub> , F <sub>0.992</sub> ) + 0.016 HF						
Run number	Δm F-Ap [μg]	m H <sub>2</sub> O [mg]	X <sub>KCl</sub>	m sec F-Ap [μg]	m HF [μg]		Calc pH	Obs pH	
<b>F-Ap_005</b>	0,80	39,60	<b>0,00</b>	0,80	0,00		6,5	6,5	
F-apatite - H <sub>2</sub> O - KCl									
1 Ca <sub>5</sub> (PO <sub>4</sub> ) <sub>3</sub> F + 0.068 H <sub>2</sub> O + 0.068 KCl			1 Ca <sub>5</sub> (PO <sub>4</sub> ) <sub>3</sub> (OH <sub>1-(x+y)</sub> , F <sub>x</sub> , Cl <sub>y</sub> ) + 0.068 OH <sup>-</sup> + (1-x) F <sup>-</sup> + 0.068H <sup>+</sup> + 0.068 K <sup>+</sup> + (0.068-y) Cl <sup>-</sup>						
			1 Ca <sub>5</sub> (PO <sub>4</sub> ) <sub>3</sub> (OH <sub>0.000</sub> , F <sub>0.932</sub> , Cl <sub>0.068</sub> ) + 0.068 HF + 0.068 KOH						
Run number	Δm F-Ap [μg]	m H <sub>2</sub> O [mg]	m KCl [mg]	X <sub>KCl</sub>	m sec F-Ap [μg]	m HF [μg]	m KOH [μg]	Calc pH	Obs pH
<b>F-Ap_012</b>	82,33	26,86	27,18	<b>0,20</b>	82,51	0,22	0,62	7,5	7,5
1 Ca <sub>5</sub> (PO <sub>4</sub> ) <sub>3</sub> F + 0.139 H <sub>2</sub> O + 0.138 KCl			1 Ca <sub>5</sub> (PO <sub>4</sub> ) <sub>3</sub> (OH <sub>1-(x+y)</sub> , F <sub>x</sub> , Cl <sub>y</sub> ) + 0.139 OH <sup>-</sup> + (1-x) F <sup>-</sup> + 0.139H <sup>+</sup> + 0.138 K <sup>+</sup> + (0.138-y) Cl <sup>-</sup>						
			1 Ca <sub>5</sub> (PO <sub>4</sub> ) <sub>3</sub> (OH <sub>0.000</sub> , F <sub>0.862</sub> , Cl <sub>0.138</sub> ) + 0.139 HF + 0.138 KOH						
Run number	Δm F-Ap [μg]	m H <sub>2</sub> O [mg]	m KCl [mg]	X <sub>KCl</sub>	m sec F-Ap [μg]	m HF [μg]	m KOH [μg]	Calc pH	Obs pH
<b>F-Ap_014</b>	101,15	13,75	38,91	<b>0,41</b>	101,61	0,56	1,56	7,5	7,5
1 Ca <sub>5</sub> (PO <sub>4</sub> ) <sub>3</sub> F + 0.254 H <sub>2</sub> O + 0.253 KCl			1 Ca <sub>5</sub> (PO <sub>4</sub> ) <sub>3</sub> (OH <sub>1-(x+y)</sub> , F <sub>x</sub> , Cl <sub>y</sub> ) + 0.253 OH <sup>-</sup> + (1-x) F <sup>-</sup> + 0.254H <sup>+</sup> + 0.253 K <sup>+</sup> + (0.253-y) Cl <sup>-</sup>						
			1 Ca <sub>5</sub> (PO <sub>4</sub> ) <sub>3</sub> (OH <sub>0.000</sub> , F <sub>0.747</sub> , Cl <sub>0.253</sub> ) + 0.254 HF + 0.253 KOH						
Run number	Δm F-Ap [μg]	m H <sub>2</sub> O [mg]	m KCl [mg]	X <sub>KCl</sub>	m sec F-Ap [μg]	m HF [μg]	m KOH [μg]	Calc pH	Obs pH
<b>F-Ap_008</b>	95,88	4,82	51,79	<b>0,72</b>	96,67	0,96	2,70	6,0	6,0

**Table 2b**  
Quench pH model of the system: Cl-apatite-H<sub>2</sub>O-KCl.

Reactants			Products									
Cl-apatite - H <sub>2</sub> O												
2 Ca <sub>5</sub> (PO <sub>4</sub> ) <sub>3</sub> Cl + 0.001 H <sub>2</sub> O			2 Ca <sub>5</sub> (PO <sub>4</sub> ) <sub>3</sub> (OH <sub>1-x</sub> , Cl <sub>x</sub> ) + (0.001 - 2(1-x)) OH <sup>-</sup> + 2(1-x) Cl <sup>-</sup> + 0.001H <sup>+</sup>									
			2 Ca <sub>5</sub> (PO <sub>4</sub> ) <sub>3</sub> (OH <sub>0.000</sub> , Cl <sub>1.000</sub> ) + 0.001 HCl									
Run number	Δm Cl-Ap [μg]	m H <sub>2</sub> O [mg]	X <sub>KCl</sub>	m sec Cl-Ap I [μg]	m HCl [μg]		Calc pH	Obs pH				
<b>Cl-Ap_007</b>	1,50	40,13	<b>0,00</b>	1,50	0,00		7,5	7,5				
Cl-apatite - H <sub>2</sub> O - KCl												
2 Ca <sub>5</sub> (PO <sub>4</sub> ) <sub>3</sub> Cl + 3.249 H <sub>2</sub> O + 0.094 KCl			1.829 Ca <sub>5</sub> (PO <sub>4</sub> ) <sub>3</sub> (OH <sub>1-x</sub> , Cl <sub>x</sub> ) + ((2*5) - (1.829*5)) Ca <sup>2+</sup> + ((2*3) - (1.829*3)) PO <sub>4</sub> <sup>3-</sup> + (2 - (1.829*x)) Cl <sup>-</sup> + 3.249H <sup>+</sup> + 3.249 OH <sup>-</sup> + 0.094 K <sup>+</sup> + 0.094 Cl <sup>-</sup>									
			1.829 Ca <sub>5</sub> (PO <sub>4</sub> ) <sub>3</sub> (OH <sub>0.790</sub> , Cl <sub>0.210</sub> ) + 0.855 Ca(OH) <sub>2</sub> + 0.513 H <sub>3</sub> PO <sub>4</sub> + 1.710 HCl + 0.094 KOH									
Run number	Δm Cl-Ap [μg]	m H <sub>2</sub> O [mg]	m KCl [mg]	X <sub>KCl</sub>	m sec Cl-Ap I [μg]	m Ca(OH) <sub>2</sub> [μg]	m HCl [μg]	m H <sub>3</sub> PO <sub>4</sub> [μg]	m KOH [μg]	Calc pH	Obs pH	
<b>Cl-Ap_023</b>	97,33	26,35	27,06	<b>0,20</b>	86,51	5,92	5,83	4,70	0,49	6,5	6,5	
2 Ca <sub>5</sub> (PO <sub>4</sub> ) <sub>3</sub> Cl + 2.389 H <sub>2</sub> O + 0.002 KCl			1.504 Ca <sub>5</sub> (PO <sub>4</sub> ) <sub>3</sub> (OH <sub>1-x</sub> , Cl <sub>x</sub> ) + 0.370 Ca <sub>5</sub> (PO <sub>4</sub> ) <sub>3</sub> (OH <sub>1-y</sub> , Cl <sub>y</sub> ) + 0.629 Ca <sup>2+</sup> + 0.377 PO <sub>4</sub> <sup>3-</sup> + (2 - (1.504*x) - (0.370*y)) Cl <sup>-</sup> + 2.389H <sup>+</sup> + 2.389 OH <sup>-</sup> + 0.002 K <sup>+</sup> + 0.002 Cl <sup>-</sup>									
			1.504 Ca <sub>5</sub> (PO <sub>4</sub> ) <sub>3</sub> (OH <sub>0.655</sub> , Cl <sub>0.345</sub> ) + 0.370 Ca <sub>5</sub> (PO <sub>4</sub> ) <sub>3</sub> (OH <sub>0.390</sub> , Cl <sub>0.610</sub> ) + 0.629 Ca(OH) <sub>2</sub> + 0.377 H <sub>3</sub> PO <sub>4</sub> + 1.258 HCl + 0.002 KOH									
Run number	Δm Cl-Ap [μg]	m H <sub>2</sub> O [mg]	m KCl [mg]	X <sub>KCl</sub>	m sec Cl-Ap I [μg]	m sec Cl-Ap II [μg]	m Ca(OH) <sub>2</sub> [μg]	m HCl [μg]	m H <sub>3</sub> PO <sub>4</sub> [μg]	m KOH [μg]	Calc pH	Obs pH
<b>Cl-Ap_025</b>	132,25	14,05	38,99	<b>0,40</b>	97,16	24,13	5,92	5,82	4,69	0,02	5,0	5,0
2 Ca <sub>5</sub> (PO <sub>4</sub> ) <sub>3</sub> Cl + 1.536 H <sub>2</sub> O + 0.000 KCl			1.919 Ca <sub>5</sub> (PO <sub>4</sub> ) <sub>3</sub> (OH <sub>1-x</sub> , Cl <sub>x</sub> ) + ((2*5) - (1.919*5)) Ca <sup>2+</sup> + ((2*3) - (1.919*3)) PO <sub>4</sub> <sup>3-</sup> + (2 - (1.919*x)) Cl <sup>-</sup> + 1.536H <sup>+</sup> + 1.536 OH <sup>-</sup> + 0.000 K <sup>+</sup> + 0.000 Cl <sup>-</sup>									
			1.919 Ca <sub>5</sub> (PO <sub>4</sub> ) <sub>3</sub> (OH <sub>0.379</sub> , Cl <sub>0.621</sub> ) + 0.404 Ca(OH) <sub>2</sub> + 0.243 H <sub>3</sub> PO <sub>4</sub> + 0.808 HCl + 0.000 KOH									
Run number	Δm Cl-Ap [μg]	m H <sub>2</sub> O [mg]	m KCl [mg]	X <sub>KCl</sub>	m sec Cl-Ap I [μg]	m Ca(OH) <sub>2</sub> [μg]	m HCl [μg]	m H <sub>3</sub> PO <sub>4</sub> [μg]	m KOH [μg]	Calc pH	Obs pH	
<b>Cl-Ap_010</b>	117,90	5,89	45,60	<b>0,65</b>	111,62	3,39	3,34	2,69	0,00	4,0	4,0	

sec F-Ap: secondary F-apatite; sec Cl-Ap I: secondary Cl-apatite (Generation I); sec Cl-Ap II: secondary Cl-apatite (Generation II).

quench material, in accordance with previous observations from similar experiments (e.g., Tropper and Manning, 2005, 2007a, 2007b; Antignano and Manning, 2008). In addition to the two types of apatite crystals, we also observed < 10 μm prismatic grains of monazite on the surface of the Durango fluorapatite starting crystals (Fig. 1e, f). These monazite grains are interpreted to result from the incongruent dissolution of the LREE-bearing Durango fluorapatite starting crystal in H<sub>2</sub>O, H<sub>2</sub>O + KCl, or H<sub>2</sub>O + NaCl, to (LREE<sup>3+</sup>)<sub>Apatite</sub> + PO<sub>4</sub><sup>3-</sup> = (LREE)PO<sub>4</sub> + dissolved solutes. Harlov and Förster (2003), Harlov et al. (2005) and Antignano and Manning (2008) also observed similar incongruent dissolution processes of Durango fluorapatite to monazite. Some of the Durango fluorapatite crystals in the system H<sub>2</sub>O + KCl, which dissolved incongruently at X<sub>KCl</sub> < 0.2 to monazite + fluid, were

weighed and then mounted for SEM imaging to investigate monazite distribution and texture (Fig. 1e, f). The crystals were cleaned ultrasonically in ethanol to dislodge the monazite, dried, re-weighed and again mounted for SEM imaging. In addition, the treatment in the ultrasonic bath completely removed the monazite grains, but the overall weights of these fluorapatite crystals nonetheless remained unchanged. The weights of residual monazite grains can hence be neglected in the solubility calculations and strictly reflect the solubility of the Durango fluorapatite and monazite, similar to the conclusions of Antignano and Manning (2008). Based on the textural observations it can be assumed that the newly- formed monazite grains nucleated during the experiment and the secondary fluorapatite crystals nucleated and grew during quench to room temperature from the experimental T, whereas the KCl

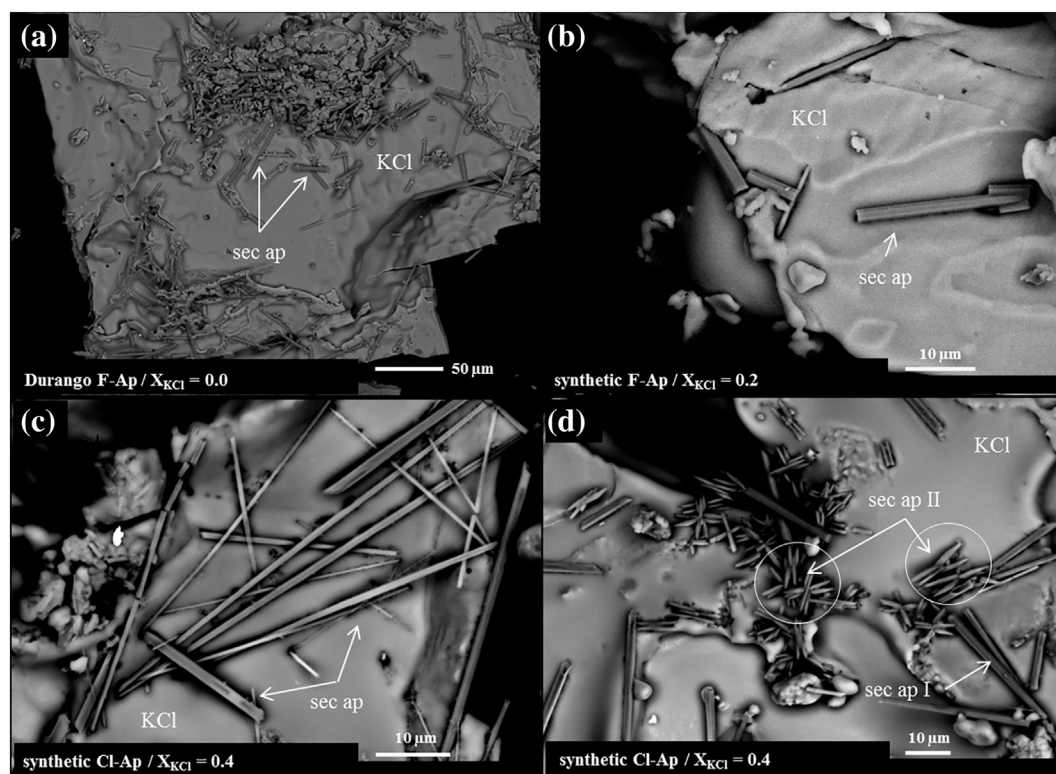


Fig. 2. SEM images of the quench material from selected experiments. (a, b, c) Hollow, prismatic, hexagonal secondary apatite (sec ap) needles which nucleate primarily in the outer capsule upon quench. (d) Two generations of secondary apatite crystals, that occur as prismatic needles (sec ap I) and stellate clusters (sec ap II).

and NaCl aggregates precipitated during drying after initial puncturing of the outer capsule. No evidence for vapor-transport of apatite was observed, unlike in some mineral-fluid systems such as calcite, rutile, and corundum (Caciagli and Manning, 2003; Tropper and Manning, 2005, 2007b) or fluorapatite in the system NaCl + H<sub>2</sub>O (Antignano and Manning, 2008).

The runtime of 24 h for each experiment at 1.0 GPa and 800 °C was sufficient to ensure significant reaction between the apatite starting crystal and solution and to attain chemical equilibrium (Antignano and Manning, 2008). Similar solubility studies on anhydrite and fluorite in the system NaCl-H<sub>2</sub>O employed the double-capsule method and demonstrated that a runtime of 24 h is sufficient for equilibration (e.g., Newton and Manning, 2005; Tropper and Manning, 2007a).

### 3.2. Fluorapatite solubility in H<sub>2</sub>O-KCl

The experimental results in the system H<sub>2</sub>O-KCl are given in Tables 1a, 1b and shown in Fig. 4. In pure H<sub>2</sub>O, the solubility of fluorapatite rises with increasing P and T (Antignano and Manning, 2008). At 800 °C and 1.0 GPa the solubilities of Durango fluorapatite and synthetic fluorapatite are 70 ± 6 ppm and 19 ± 3 ppm respectively. In comparison with the experimental results investigated by Antignano and Manning (2008), the solubility of the Durango fluorapatite in pure H<sub>2</sub>O is slightly lower (61 ± 8 ppm). The solubilities of the Durango fluorapatite and synthetic fluorapatite are similar in H<sub>2</sub>O-KCl fluids. Results indicate an increase in dissolved fluorapatite concentration with rising X<sub>KCl</sub> to near sylvite saturation from 1124 ± 11 ppm (X<sub>KCl</sub> = 0.10) and 1210 ± 6 ppm (X<sub>KCl</sub> = 0.10) to 2073 ± 6 ppm (X<sub>KCl</sub> = 0.50) and 2123 ± 6 ppm (X<sub>KCl</sub> = 0.52) (Table 1a) (Fig. 4). At X<sub>KCl</sub> > 0.5, the solubilities of the Durango fluorapatite and synthetic fluorapatite decrease with increasing KCl from 2073 ± 6 ppm (X<sub>KCl</sub> = 0.50) and 2123 ± 6 ppm (X<sub>KCl</sub> = 0.52) to 1665 ± 5 ppm (X<sub>KCl</sub> = 0.65) and 1691 ± 7 ppm (X<sub>KCl</sub> = 0.72) (Fig. 4). The data can be fit using a second-degree polynomial function to describe fluorapatite solubility as

a function of KCl mole fraction (X<sub>KCl</sub>) at 1.0 GPa and 800 °C (Fig. 4). The following fit equations can be proposed:

$$m_{F-ap}(\text{Dur.}) = -10,475 X_{KCl}^2 + 9209 X_{KCl} + 70 \quad (1)$$

$$m_{F-ap}(\text{syn.}) = -9128 X_{KCl}^2 + 8818 X_{KCl} + 19 \quad (2)$$

where  $m_{F-ap}(\text{Dur.})$  is the solubility of the Durango fluorapatite in ppm,  $m_{F-ap}(\text{syn.})$  is the solubility of synthetic fluorapatite in ppm, and X<sub>KCl</sub> is the mole fraction of KCl.

The quench pH of the aqueous solutions in the system fluorapatite-H<sub>2</sub>O-KCl was found to vary from 6.0–7.5 with a clear correlation with the starting KCl mole fraction (X<sub>KCl</sub>), while the runs in pure H<sub>2</sub>O showed quench pH values of ~6.5 (Table 1a). The runs with X<sub>KCl</sub> = 0.1–0.4 showed slightly basic quench pH values of ~7.5. The runs with the highest mole fractions of X<sub>KCl</sub> = 0.5–0.7 showed neutral-slightly acidic quench pH values of ~7.0–6.0 (Table 1a).

### 3.3. Chlorapatite solubility in H<sub>2</sub>O-KCl

At 800 °C and 1.0 GPa, the solubility of synthetic chlorapatite in pure H<sub>2</sub>O is 37 ± 6 ppm (Table 1a). Overall, the solubility of synthetic chlorapatite is much higher than the solubilities of natural and synthetic fluorapatite in the system H<sub>2</sub>O-KCl at 800 °C, 1.0 GPa. It also shows an increase in dissolved chlorapatite concentration with rising X<sub>KCl</sub> to near sylvite saturation from 1495 ± 6 ppm (X<sub>KCl</sub> = 0.11) to 2590 ± 20 ppm (X<sub>KCl</sub> = 0.50) (Table 1a, Fig. 4). At X<sub>KCl</sub> > 0.5, the solubility of synthetic chlorapatite decreases with increasing KCl from 2590 ± 20 ppm (X<sub>KCl</sub> = 0.50) to 2284 ± 6 ppm (X<sub>KCl</sub> = 0.65). Similar to the fluorapatite solubilities a second-degree polynomial function was used to describe the solubility as a function of the KCl mole fraction (X<sub>KCl</sub>) at 1.0 GPa and 800 °C (Fig. 4). A fit to the data can be described by:

$$m_{Cl-ap}(\text{syn.}) = -12,187 X_{KCl}^2 + 11,278 X_{KCl} + 37 \quad (3)$$

where  $m_{Cl-ap}(\text{syn.})$  is the solubility of synthetic chlorapatite in ppm and

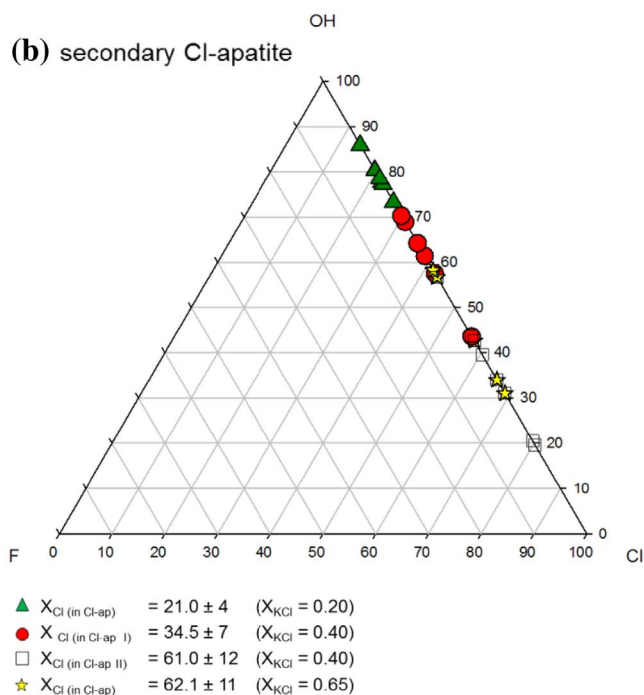
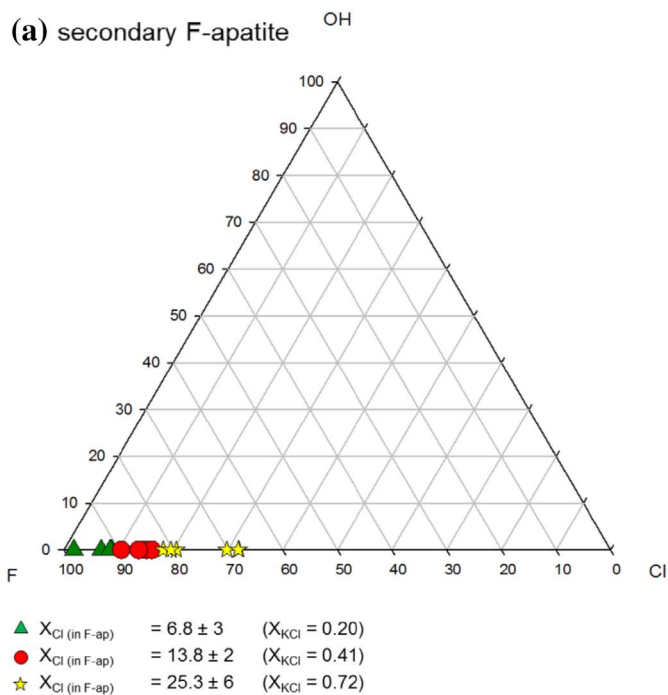


**Fig. 3.** Partitioning behaviour of chlorine in (a) secondary F-apatite and (b) secondary Cl-apatite in the system H<sub>2</sub>O-KCl. (b) In the system Cl-apatite – H<sub>2</sub>O – KCl at a mole fraction of X<sub>KCl</sub> = 0.4 exist two secondary apatite generations (Cl-ap I, Cl-ap II) with different chlorine contents.

X<sub>KCl</sub> is the mole fraction of KCl.

The quench pH of the aqueous solutions in the system chlorapatite-H<sub>2</sub>O-KCl show much higher variation from 3.5–7.5 with a clear correlation with the starting KCl mole fraction (X<sub>KCl</sub>), while the runs in pure H<sub>2</sub>O showed quench pH values of ~7.5 (Table 1a). At X<sub>KCl</sub> > 0.1, the quench pH values decrease with increasing KCl from a slightly basic pH of 7.5 (X<sub>KCl</sub> = 0.11) to a strong acidic pH of 3.5 and 4.0 (X<sub>KCl</sub> = 0.50 and X<sub>KCl</sub> = 0.65) (Table 1a).

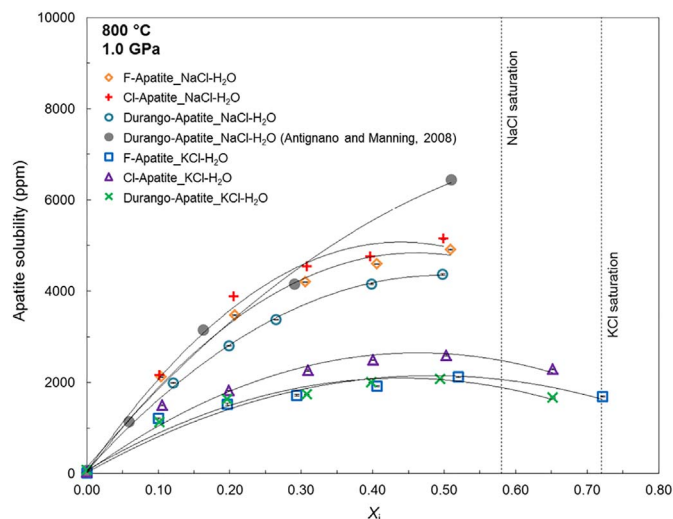


**Fig. 4.** Apatite solubility versus the mole fraction of KCl and NaCl (X<sub>i</sub>) at 800 °C and 1.0 GPa. The error bars are 2σ and are calculated based on the weighing uncertainties. The solid lines are the fitted solubilities from Eqs. (1) (Durango-ap-KCl-H<sub>2</sub>O); (2) (F-ap-KCl-H<sub>2</sub>O); (3) (Cl-ap-KCl-H<sub>2</sub>O); (4) (Durango-ap-NaCl-H<sub>2</sub>O); (5) (F-ap-NaCl-H<sub>2</sub>O) and (6) Cl-ap-NaCl-H<sub>2</sub>O. Results of Antignano and Manning (2008) from Durango-ap-NaCl-H<sub>2</sub>O at 800 °C and 1.0 GPa are shown for comparison.

### 3.4. Fluorapatite solubility in H<sub>2</sub>O-NaCl

At 800 °C and 1.0 GPa the solubilities of the Durango fluorapatite and synthetic fluorapatite in H<sub>2</sub>O-NaCl fluids indicate an increase in the dissolved fluorapatite concentration with rising X<sub>NaCl</sub> to near halite saturation from 1985 ± 7 ppm (X<sub>NaCl</sub> = 0.12) and 2115 ± 3 ppm (X<sub>NaCl</sub> = 0.10) to 4367 ± 8 ppm (X<sub>NaCl</sub> = 0.50) and 4909 ± 6 ppm (X<sub>NaCl</sub> = 0.51) (Table 1b, Fig. 4). In this case a second-degree polynomial function describes the fluorapatite solubilities as a function of the NaCl mole fraction (X<sub>NaCl</sub>) at 1.0 GPa and 800 °C (Fig. 4). The following fit equations can be proposed:

$$m_{F-ap}(\text{Dur.}) = -17,333 X_{NaCl}^2 + 17,220 X_{NaCl} + 70 \quad (4)$$

$$m_{F-ap}(\text{syn.}) = -22,680 X_{NaCl}^2 + 20,909 X_{NaCl} + 19 \quad (5)$$

where m<sub>F-ap</sub>(Dur.) is the solubility of Durango fluorapatite in ppm, m<sub>F-ap</sub>(syn.) is the solubility of synthetic fluorapatite in ppm and X<sub>NaCl</sub> is the mole fraction of NaCl.

It can also be seen from Fig. 4 that the solubilities of the synthetic fluorapatite are slightly higher than the solubilities of the Durango fluorapatite in the system H<sub>2</sub>O-NaCl. This is in contrast to the H<sub>2</sub>O-KCl system where apatite solubilities are considerably lower (see also Antignano and Manning, 2008). In comparison with the experimental results by Antignano and Manning (2008), the solubilities of the Durango fluorapatite in H<sub>2</sub>O-NaCl fluids at 800 °C, 1.0 GPa are similar up to X<sub>NaCl</sub> = 0.3 (Table 1b, Fig. 4). However, at X<sub>NaCl</sub> > 0.3, especially at X<sub>NaCl</sub> = 0.5, the calculated solubility of the Durango fluorapatite from Antignano and Manning (2008) is much greater than our estimation of the Durango and synthetic fluorapatite solubilities. The quench pH of the aqueous solutions in the system Durango fluorapatite-H<sub>2</sub>O-NaCl was found to vary from 4.0–8.0 with a clear correlation with the starting NaCl mole fraction (X<sub>NaCl</sub>). At X<sub>NaCl</sub> > 0.1 the quench pH values decrease with increasing NaCl from a neutral pH of 7.0 (X<sub>NaCl</sub> = 0.20) to a strong acidic pH of 4.0 (X<sub>NaCl</sub> = 0.40). At X<sub>NaCl</sub> > 0.4, the quench pH values increase with increasing NaCl from a strong acidic pH of 4.0 (X<sub>NaCl</sub> = 0.40) to an acidic pH of 4.5 (X<sub>NaCl</sub> = 0.50) (Table 1b). The quench pH values of the synthetic fluorapatite-H<sub>2</sub>O-NaCl aqueous solutions were found to vary from 3.0–6.5 with a clear correlation with the starting NaCl mole fraction (X<sub>NaCl</sub>) (Table 1b).

### 3.5. Chlorapatite solubility in H<sub>2</sub>O-NaCl

The solubilities of synthetic chlorapatite are higher than the solubilities of synthetic fluorapatite and Durango fluorapatite in the system H<sub>2</sub>O-NaCl at 800 °C, 1.0 GPa, but indicate an increase in the dissolved chlorapatite concentration with rising X<sub>NaCl</sub> to near halite saturation from 2162 ± 24 ppm (X<sub>NaCl</sub> = 0.10) to 5144 ± 14 ppm (X<sub>NaCl</sub> = 0.50) (Table 1b, Fig. 4). A second-degree polynomial function describes the chlorapatite solubilities as a function of the NaCl mole fraction (X<sub>NaCl</sub>) at 1.0 GPa and 800 °C (Fig. 4):

$$m_{\text{Cl-ap (syn.)}} = -26,092 X_{\text{NaCl}}^2 + 22,928 X_{\text{NaCl}} + 37 \quad (6)$$

where m<sub>Cl-ap (syn.)</sub> is the solubility of synthetic chlorapatite in ppm and X<sub>NaCl</sub> is the mole fraction of NaCl.

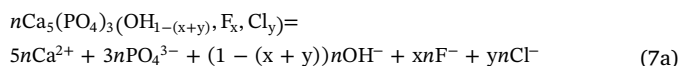
The quench pH of the aqueous solutions in the system chlorapatite-H<sub>2</sub>O-NaCl was found to vary from 3.5–7.5 with a clear correlation with the starting NaCl mole fraction (X<sub>NaCl</sub>). At X<sub>NaCl</sub> > 0.1 the quench pH values decrease with increasing NaCl from a neutral pH of 7.5 (X<sub>NaCl</sub> = 0.10) to an acidic pH of 3.5 (X<sub>NaCl</sub> = 0.50) (Table 1b).

## 4. Discussion

### 4.1. Apatite solubility as a function of X<sub>i</sub> at 800 °C and 1.0 GPa

At similar P (1.0 GPa), T (800 °C), and runtime (24 h), the solubilities of the Durango fluorapatite (70 ppm, this study) (62 ppm, Antignano and Manning, 2008), synthetic F<sup>-</sup> (19 ppm) and chlorapatite (37 ppm) in pure H<sub>2</sub>O are much lower than that of the other Ca compounds that have been studied. These include fluorite (952 ppm, runtime = 24 h; Tropper and Manning, 2007a), wollastonite (2622 ppm, runtime = 17 h; Newton and Manning, 2006), anhydrite (4543 ppm, runtime = 18 h; Newton and Manning, 2005), and calcite (11,605 ppm, runtime = 10 h; Newton and Manning, 2002). The low solubility of apatite in pure H<sub>2</sub>O demonstrates that it is the most refractory of these Ca-bearing minerals commonly found in high-grade metamorphic rocks, if the pore fluids consist of dilute aqueous solutions (Antignano and Manning, 2008).

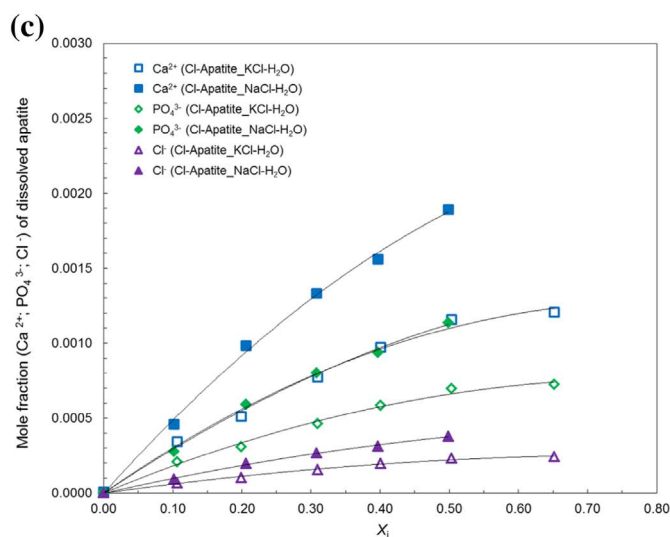
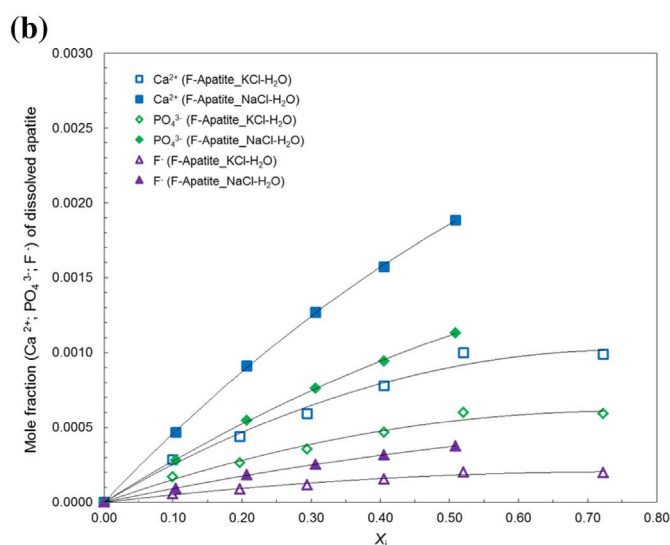
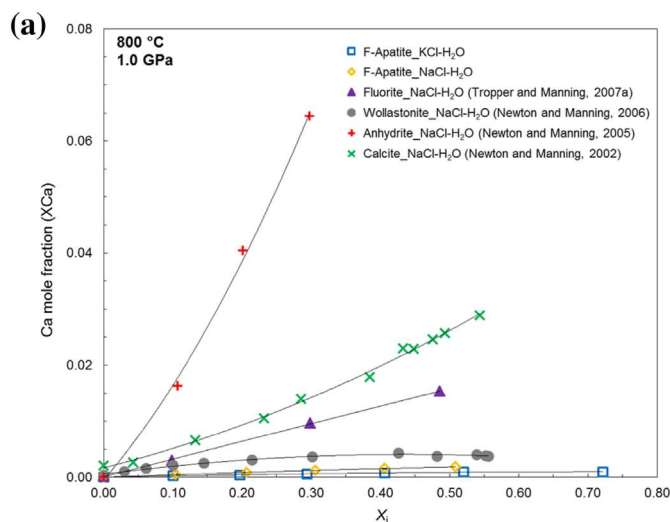
Fig. 5a shows the comparison between the predicted solubility of apatite with that of fluorite (Tropper and Manning, 2007a), wollastonite (Newton and Manning, 2006), anhydrite (Newton and Manning, 2005) and calcite (Newton and Manning, 2002) at 800 °C and 1.0 GPa. Here, the concentration scale represents the Ca mole fraction of the Ca-bearing minerals in solution (X<sub>Ca</sub>) vs. the mole fraction of KCl and NaCl (X<sub>i</sub>), assuming for simplicity that apatite composition is stoichiometric Ca<sub>5</sub>(PO<sub>4</sub>)<sub>3</sub>F. As with the other Ca-bearing minerals, the Ca mole fraction in apatite-equilibrated H<sub>2</sub>O-KCl and H<sub>2</sub>O-NaCl fluids rises with increasing KCl or NaCl concentration (Fig. 5a). Also the Ca mole fraction at apatite saturation in H<sub>2</sub>O-KCl fluids is lower than in H<sub>2</sub>O-NaCl fluids. However, at any X<sub>NaCl</sub> at 800 °C and 1.0 GPa, the Ca solubilities at apatite saturation are much lower than in fluids coexisting with fluorite, wollastonite, anhydrite, or calcite (Fig. 5a). Fig. 5b and c show the mole fractions of dissolved apatite components (Ca<sup>2+</sup>, PO<sub>4</sub><sup>3-</sup>, F<sup>-</sup>, Cl<sup>-</sup>) in the fluid as a function of X<sub>KCl</sub> and X<sub>NaCl</sub>. Assuming the following dissociation reaction:



the mole fractions of the apatite components (with X<sub>OH<sup>-</sup></sub> = 0.0) can be calculated via the formula:

$$\begin{aligned} X_i (i = \text{Ca}^{2+}, \text{PO}_4^{3-}, \text{F}^-, \text{Cl}^-) = \\ n_i (i = \text{Ca}^{2+}, \text{PO}_4^{3-}, \text{F}^-, \text{Cl}^-) / n_i (i = \text{Ca}^{2+}, \text{PO}_4^{3-}, \text{F}^-, \text{Cl}^-) + n(\text{H}_2\text{O} + \text{KCl}) \end{aligned} \quad (7b)$$

or



(caption on next page)

**Fig. 5.** a. Comparison of the predicted solubility of F-apatite with that of fluorite (Tropper and Manning, 2007a), wollastonite (Newton and Manning, 2006), anhydrite (Newton and Manning, 2005) and calcite (Newton and Manning, 2002). Comparison of solubility calculated as mole fraction of Ca in solution vs. the mole fraction of KCl and NaCl ( $X_i$ ). b. Comparison of the mole fractions of the dissolved F-apatite components ( $\text{Ca}^{2+}$ ,  $\text{PO}_4^{3-}$ ,  $\text{F}^-$ ) in the fluid as a function of  $X_{\text{KCl}}$  and  $X_{\text{NaCl}}$ . c. Comparison of the mole fractions of the dissolved Cl-apatite components ( $\text{Ca}^{2+}$ ,  $\text{PO}_4^{3-}$ ,  $\text{Cl}^-$ ) in the fluid as a function of  $X_{\text{KCl}}$  and  $X_{\text{NaCl}}$ .

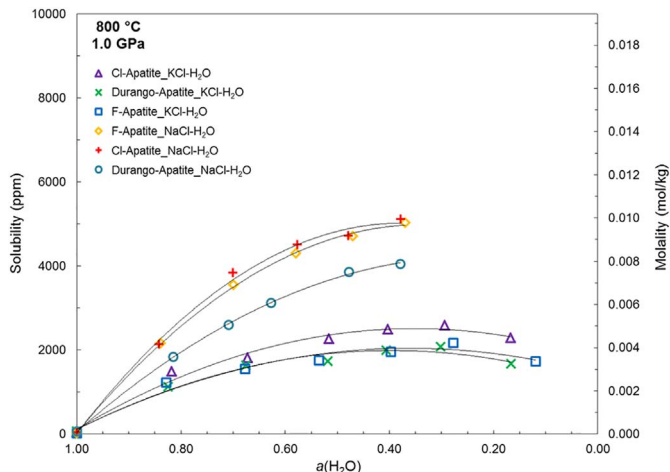


**Fig. 6.** The relation between the solubility and the molality of apatite vs. the activity of  $\text{H}_2\text{O}$  at 800 °C and 1.0 GPa.

$$X_i (i = \text{Ca}^{2+}, \text{PO}_4^{3-}, \text{F}^-, \text{Cl}^-) =$$

$$n_i (i = \text{Ca}^{2+}, \text{PO}_4^{3-}, \text{F}^-, \text{Cl}^-) / n_i (i = \text{Ca}^{2+}, \text{PO}_4^{3-}, \text{F}^-, \text{Cl}^-) + n(\text{H}_2\text{O} + \text{NaCl}) \quad (7c)$$

The components of fluorapatite (Fig. 5b) and chlorapatite (Fig. 5c) are more soluble in  $\text{H}_2\text{O}$ -NaCl fluids than in  $\text{H}_2\text{O}$ -KCl fluids. Based on the chemical formula of apatite ( $\text{Ca}_5(\text{PO}_4)_3(\text{F}, \text{Cl})$ ), the amounts of dissolved  $\text{Ca}^{2+}$  and  $\text{PO}_4^{3-}$  are 5 times and 3 times greater, respectively, than the amounts of  $\text{F}^-$  or  $\text{Cl}^-$  in the  $\text{H}_2\text{O}$ -NaCl and  $\text{H}_2\text{O}$ -KCl fluid. The mole fractions of the dissolved components rise with increasing KCl or NaCl concentration and each of them shows the same positive trend.

Fig. 6 shows the relation between the solubility (primary vertical  $y_1$ -axis) and the molality (secondary vertical  $y_2$ -axis) of apatite vs. the activity of  $\text{H}_2\text{O}$ . The molality of the apatite is reported in mol/kg, and is calculated from the amount of substance ( $n_{\text{Apatite}}$ ) divided by the mass of  $\text{H}_2\text{O} + \text{KCl}$  or  $\text{H}_2\text{O} + \text{NaCl}$  in concentrated KCl and NaCl solutions were calculated at 800 °C, 1.0 GPa and at KCl or NaCl concentration up to sylvite or halite saturation. The  $\text{H}_2\text{O}$ , KCl and NaCl activities were evaluated using the technique outlined in Aranovich and Newton (1996, 1997). At 1.0 GPa, solutions closely approach an ideal fused salt mixture, where the activities of  $\text{H}_2\text{O}$ , KCl and NaCl correspond to an ideal activity formulation (Aranovich and Newton, 1996). The low  $\text{H}_2\text{O}$  activity at high pressures in concentrated KCl and NaCl solutions indicates that such solutions should be feasible as chemically active fluids capable of coexisting with solid rocks in many processes of deep crustal and upper mantle metamorphism and metasomatism (Aranovich and Newton, 1996).

The effect of KCl or NaCl on apatite solubility can be assessed from the log-ratios  $X_{\text{Ca}}^*/X_{\text{Ca}}$ , where  $X_{\text{Ca}}^*$  is the Ca mole fraction of apatite in pure  $\text{H}_2\text{O}$  (Fig. 7).  $\text{H}_2\text{O}$ -KCl and  $\text{H}_2\text{O}$ -NaCl fluids enhance the solubility of apatite to an extent similar to anhydrite and fluorite, but to a much greater degree than wollastonite and calcite (Fig. 7). The trends observed in Fig. 7 indicate that  $\text{H}_2\text{O}$  is not the only component involved as a solution mechanism in the dissolution of the Ca salts (Newton and Manning, 2002). In this case, a decrease in the  $\text{H}_2\text{O}$  activity, associated with an increase in the NaCl and KCl concentration, would inhibit mineral solubility in concentrated solutions similar to what is seen for

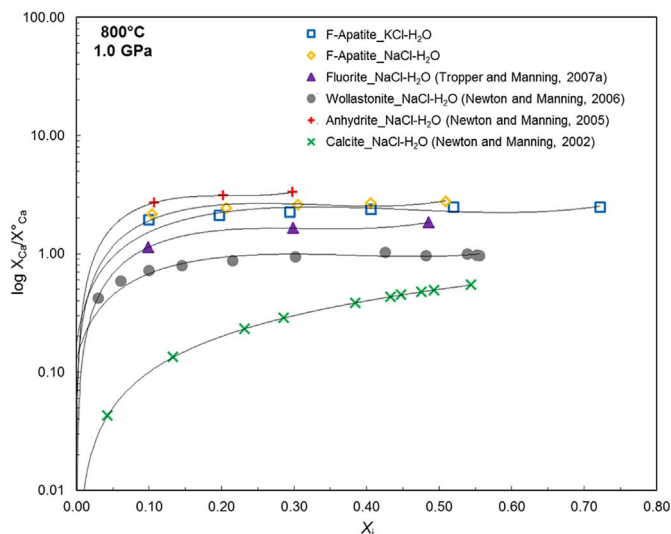
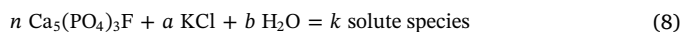


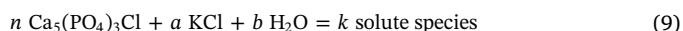
**Fig. 7.** Comparison of the enhancement of solubility of F-apatite with that of fluorite (Tropper and Manning, 2007a), wollastonite (Newton and Manning, 2006), anhydrite (Newton and Manning, 2005) and calcite (Newton and Manning, 2002), as determined from the log-ratio of predicted solubility ( $X_{\text{Ca}}$ ) divided by that in  $\text{H}_2\text{O}$  ( $X_{\text{Ca}}^*$ ) vs. the mole fraction of KCl and NaCl ( $X_i$ ).

quartz, wollastonite, or corundum (Newton and Manning, 2006). The solubilities of apatite in KCl- $\text{H}_2\text{O}$  and NaCl- $\text{H}_2\text{O}$  fluids at 800 °C, 1.0 GPa increase with rising  $X_{\text{KCl}}$  and  $X_{\text{NaCl}}$ , but the dependence of the relative solubility on the salinity differs (Fig. 7). This indicates that apatite is more soluble in NaCl- $\text{H}_2\text{O}$  fluids than in KCl- $\text{H}_2\text{O}$  fluids over the investigated range of  $X_{\text{KCl}}$  and  $X_{\text{NaCl}}$ .

To obtain information on the interaction of fluor- and chlorapatite, especially with pure  $\text{H}_2\text{O}$  and KCl +  $\text{H}_2\text{O}$  solutions, the following generalized dissolution reactions may be written (Newton and Manning, 2006, 2010; Tropper and Manning, 2011):



or



where  $n$  is the number of moles of apatite, and  $a$  and  $b$  are the number of moles of KCl and  $\text{H}_2\text{O}$  consumed to produce  $k$  moles of solutes per mole of orthophosphate dissolved. The relative molar proportions of KCl and  $\text{H}_2\text{O}$  in Eqs. (8) and (9) were evaluated using the technique outlined in Newton and Manning (2006, 2010) via the equation:

$$X_{\text{KCl}}^* = \frac{a}{a + b} \quad (10)$$

The  $k$  moles of solutes per mole of orthophosphate were calculated assuming complete dissociation to  $n$  ( $5 \text{Ca}^{2+} + 3 \text{PO}_4^{3-} + \text{F}^- + (\text{Cl}^-) + a \text{K}^+ + a \text{Cl}^- + b \text{H}^+ + b \text{OH}^-$  (Bradley, 1962; Aranovich and Newton, 1996; Newton and Manning, 2006). Fig. 8a and b show the variations in the relative solubility enhancements of synthetic fluorapatite and chlorapatite, and Durango fluorapatite, expressed as a solute mole fraction for a given  $X_{\text{KCl}}$  and  $X_{\text{NaCl}}$  relative to that in pure  $\text{H}_2\text{O}$  ( $X^*$ ). The ratio  $X/X^*$  thus represents the magnitude of solubility enhancement by a given KCl or NaCl mole fraction. Values of  $\log X/X^*$ , especially for synthetic fluorapatite in KCl solutions, rise with  $X_{\text{KCl}}$  over the investigated range to a maximum at  $X_{\text{KCl}} \sim 0.30$  (Fig. 8a). This implies that the activities of KCl and  $\text{H}_2\text{O}$  significantly influence apatite solubility. In Eq. (10), the KCl mole fraction ( $X_{\text{KCl}} = 0.30$ ), at which the maximum solubility occurs, defines the ratio of  $a$  to  $b$  and implies that  $a = 0.035$  and  $b = 0.080$  (Fig. 8a). A simple chemical equilibrium that could account for this relationship is:

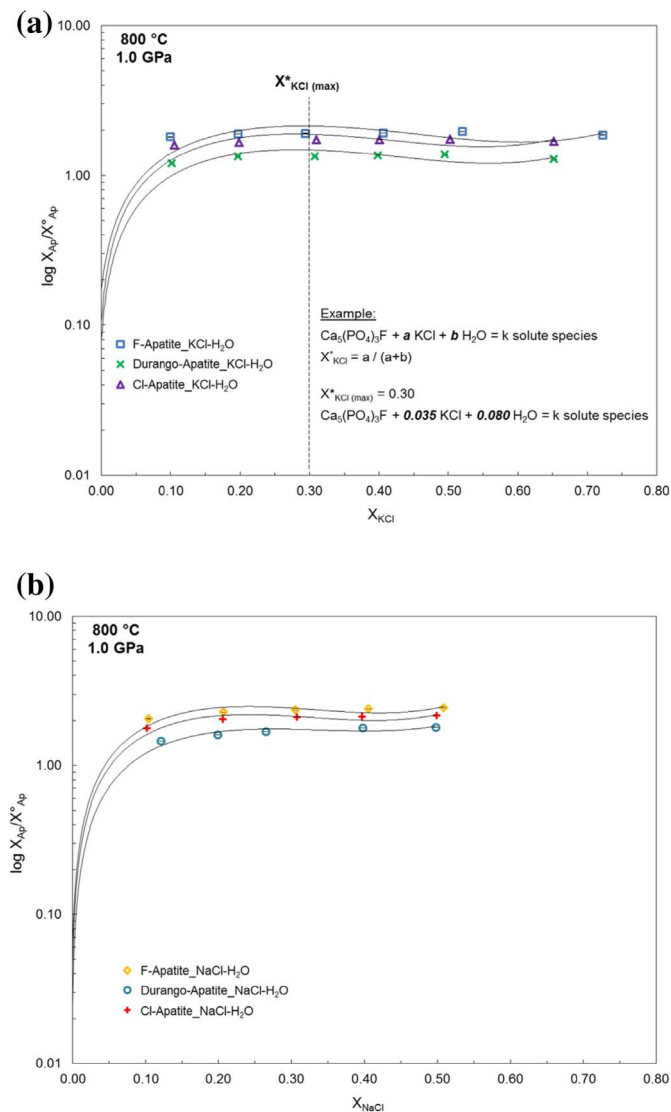
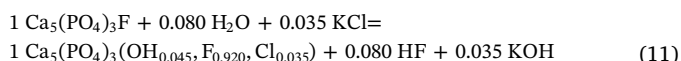
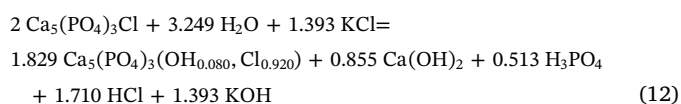


**Fig. 8.** a. Comparison of the enhancement of solubility of synthetic F-apatite with that of synthetic Cl-apatite and Durango F-apatite, as determined from the log-ratio of predicted apatite solubility ( $X_{Ap}$ ) divided by that in  $H_2O$  ( $X_{Ap}^{\circ}$ ) vs. the mole fraction of KCl ( $X_{KCl}$ ). The KCl mole fraction ( $X_{KCl} = 0.30$ ) at which the maximum solubility of synthetic F-apatite occurs, defines the ratio of a to b and suggests that  $a = 0.035$  and  $b = 0.080$ . b. Comparison of the enhancement of solubility of synthetic F-apatite with that of synthetic Cl-apatite and Durango F-apatite, as determined from the log-ratio of predicted apatite solubility ( $X_{Ap}$ ) divided by that in  $H_2O$  ( $X_{Ap}^{\circ}$ ) vs. the mole fraction of NaCl ( $X_{NaCl}$ ).



The dissolution products in the KCl-bearing fluids are newly formed secondary apatite, HF, and KOH (Eq. (11)).

Similar to what is seen for the synthetic fluorapatite, the values of  $\log X/X^{\circ}$  for the synthetic chlorapatite rise with increasing  $X_{KCl}$  over the investigated range to a maximum at  $X_{KCl} \sim 0.30$  (Fig. 8a). The KCl mole fraction ( $X_{KCl} = 0.30$ ) for the observed maximum solubility defines the ratio shown by Eq. (10) to be  $a = 1.393$  and  $b = 3.249$ :



In the system chlorapatite-KCl- $H_2O$  the dissolution products are newly formed secondary apatite (Table 2b, Fig. 3b),  $Ca(OH)_2$ ,  $H_3PO_4$ , HCl and KOH (Eq. (12)).

#### 4.2. Quantitative modeling of observed quench pH's

A comprehensive step-by-step procedure is used to derive a self-consistent quench pH model for the system apatite-KCl- $H_2O$ , which is based on the amount of limiting reactant to calculate the amount of products (Tables 2a, 2b). The measured and calculated pH of the solution is a measure of the molar concentration of hydrogen ions in the solution and as such represents a measure of the acidity or basicity of the system. The influence of the quench pH for the apatite-KCl- $H_2O$  aqueous solution (with different  $X_{KCl}$ ) is calculated by using a set of acid-base reactions occurring assuming local equilibrium. This method allows understanding the internal pH dynamics of an aqueous system during quenching. Since direct measurements of pH as a function of P and T, and the use of a fully buffered mineral assemblage to ensure a certain pH value at P and T, are not feasible with the experimental set-up of the single crystal dissolution method, quantitative modeling of the obtained solubilities can only be done indirectly by using the quench pH. Although the quench pH is not related to the  $H^+$  activity at the experimental conditions at 1.0 GPa and 800 °C, it is still a sensitive measure of the charge balance in the quench. By determining the quench pH of the experiment (Tables 2a, 2b), information on the composition and quantity of the dissolved fluid species can be obtained. Two examples are given in Appendix I. Tables 2a and 2b give the quench pH for each experiment and it is noteworthy that the quench pH is more acidic in the system apatite- $H_2O$ -NaCl than in the system apatite- $H_2O$ -KCl. The difference in quench pH between  $H_2O$ -NaCl and  $H_2O$ -KCl also correlates well with significantly higher apatite solubilities in the system  $H_2O$ -NaCl. This observation is also supported by recent experimental investigations on monazite solubility in  $H_2O$ -Na-K-Cl-F- $CO_2$  by Zhou et al. (2016) who also reported higher monazite solubility in the presence of NaCl. Up to now almost all high P-T solubility measurements were done in the system  $H_2O$ -NaCl (see Newton and Manning, 2010) but clearly more systematic investigations on the influence of the composition of saline fluids on the solubility behaviour of minerals are needed.

#### 5. Geological implications

Saline fluids can be produced or concentrated by a variety of mechanisms (Newton et al., 1998; Yardley and Graham, 2002), including inheritance of an originally saline connate fluid, dissolution of salts of sedimentary origin,  $H_2O$  loss by preferential partitioning into hydrous minerals during retrograde metamorphism or into hydrous silicate liquids during melting and infiltration of externally derived fluids exsolved from hydrous magma. Apatite represents a very common accessory mineral in igneous and metamorphic rocks that is widely used to evaluate petrogenetic processes (e.g., Piccoli and Candela, 2002; Spear and Pyle, 2002). Studying apatite's composition offers opportunities to monitor a wide range of fluid-induced processes during high-grade metasomatism in the amphibolite- as well as granulite-facies (e.g., Harlov and Förster, 2002; Harlov et al., 2006; Newton and Manning, 2010; Harlov, 2012; Aranovich et al., 2014; Manning and Aranovich, 2014; Harlov, 2015; Kusebauch et al., 2015a, 2015b). The high experimental solubility of apatite in brines as shown in this study offers an explanation for the formation of apatite-monazite textures associated with metasomatic alteration of apatite during charnockitisation (e.g., Harlov, 2012; Harlov and Förster, 2002; Hansen and Harlov, 2007, 2009) and accompanying experimental work regarding metasomatic alteration of apatite to monazite (e.g., Harlov et al., 2002; Harlov and Förster, 2003; Harlov et al., 2005). This metasomatic alteration is associated with infiltrating NaCl- and KCl-bearing fluids during peak metamorphism as well as post peak and possibly more  $H_2O$ -rich fluids during uplift and cooling. With respect to the formation of large-scale ore deposits the results from these experiments can also be related to the extensive metasomatic alteration and remobilization of apatite in iron-oxide-apatite (IOA) deposits (Harlov et al., 2002; Taghipour et al.,

2015; Jonsson et al., 2016; Harlov et al., 2016). With respect to mantle metasomatism our experiments can be thought as a model representation of metasomatic processes in the mantles of Earth and other terrestrial planets (e.g., O'Reilly and Griffin, 2000; Patiño Douce and Roden, 2006) where apatite-rich veins and pockets in the Phanerozoic lithospheric mantle frequently occur (O'Reilly and Griffin, 2000). In subduction-zone settings, apatite in vein assemblages and as daughter minerals in fluid inclusions testifies to the mobility of its essential constituents in high-pressure fluids (e.g., Selverstone et al., 1992; Philippot and Selverstone, 1991; Franz et al., 2001). The P-T conditions of the experiments also represent conditions at the base of the lithospheric mantle wedge in subduction zones where large-scale fluid flow associated with recycling of the Earth's halogens occurs with respect to halogen concentrations and isotopic compositions (e.g., John et al., 2011). From a layered descending oceanic plate, fluids liberated during slab deserpentinization pass through and interact with the overlying crustal and sedimentary sequence of the descending slab before they reach the mantle wedge. During this process the halogen concentration in the fluids increases before they interact with the minerals of the mantle wedge and John et al. (2011) show that halogen concentrations and ratios and Cl isotope data indicate halogen input from sedimentary reservoirs during shallow serpentinization and that fluids exchanged chemically with sediments. The interaction between saline brines and the mineral assemblages of the mantle wedge is manifested by halogen incorporation into mantle minerals and a number of recent studies investigated the possibility of halogen incorporation into nominally halogen-free mantle minerals (e.g., John et al., 2011; Bernini et al., 2013). John et al. (2011) have shown that the halogen compositions of the analyzed serpentinite samples indicate input from seawater and sedimentary sources during initial serpentinization of either subducting lithospheric mantle during slab bending or forearc mantle by uprising slab fluids. Experimental investigations by Bernini et al. (2013) have

shown that F incorporation is several magnitudes higher than Cl incorporation into mantle minerals and that halogen incorporation is independent of fluid salinity. In addition to elevated halogen contents of mantle wedge minerals there is strong evidence from the Cl/H<sub>2</sub>O ratios of primitive arc basalts that the fluids dissolved in the magma in the zone of melting have elevated salinities (e.g., Johnson et al., 2009). The fluid salinities inferred from the Cl/H<sub>2</sub>O ratio of arc basalts are much higher than the initial salinities expected for fluids released from a dehydrating slab and the source of both water and chlorine in the slab is seawater, which interacted with sediments and igneous rocks where dissolution of apatite might occur.

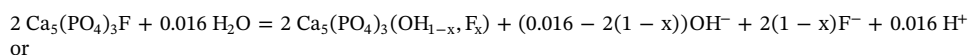
The important role of saline fluids in high-grade metasomatic mass transfer has only recently gained experimental attention, but a growing body of solubility data offers insights into interactions between salty fluids and minerals at moderate to high *P* and high *T* (e.g., Newton and Manning, 2010; Manning and Aranovich, 2014). The data point to the conclusion that alkali halide brine components of deep crustal and upper-mantle fluids represent powerful solvents capable of significant mass transfer—not just of metals, but of nearly all major rock forming oxides. This behaviour helps explain petrologic observations from a wide range of deep geologic environments.

### Acknowledgments

The financial support from the Institute of Mineralogy and Petrography, University of Innsbruck is greatly acknowledged. Martina Tribus is thanked for her help with the SEM and Hannes Witting for his help in the high-pressure laboratory. The manuscript was significantly improved by reviews by John Mavrogenes, and an anonymous reviewer. Klaus Mezger is gratefully acknowledged for the editorial handling of the manuscript.

### Appendix I

Based on the limiting reactant approach, the following dissolution reactions in the system fluorapatite-KCl-H<sub>2</sub>O can be proposed (Table 2a):  
fluorapatite-H<sub>2</sub>O ( $X_{\text{KCl}} = 0.00$  and  $\text{pH} = 6.5$ )



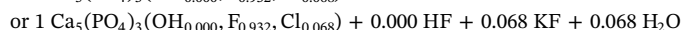
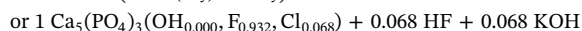
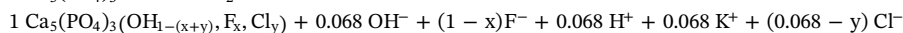
or



(13)

The dissolution reaction in pure H<sub>2</sub>O ( $X_{\text{KCl}} = 0.00$ ) is characterized with an excess of HF in the aqueous solution that produces the slightly acidic pH of 6.5 (Table 2a).

fluorapatite-H<sub>2</sub>O-KCl ( $X_{\text{KCl}} = 0.20$  and  $\text{pH} = 7.5$ )

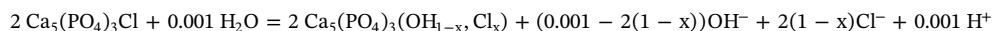


(14)

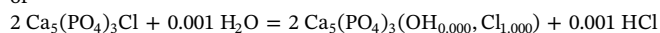
The pH for pure H<sub>2</sub>O and KCl in solution with the H<sub>2</sub>O are both neutral, since dissociation of water produces equal numbers of both ions (e.g. Petrucci et al., 2006; Mortimer et al., 2015). The dissolution reaction with  $X_{\text{KCl}} = 0.20$  is defined as a neutralization reaction, in which the acid (HF) and the base (KOH) react to form H<sub>2</sub>O and KF and the H<sup>+</sup> combines with OH<sup>-</sup> ions to generate H<sub>2</sub>O. The neutralization of a strong acid and strong base has a pH equal to 7. The resulting pH when a strong base (KOH) reacts with a weak acid (HF) will be > 7.

The dissolution reactions in the system chlorapatite-KCl-H<sub>2</sub>O can be represented by the following equations (Table 2b):

chlorapatite-H<sub>2</sub>O ( $X_{\text{KCl}} = 0.00$  and  $\text{pH} = 7.5$ )



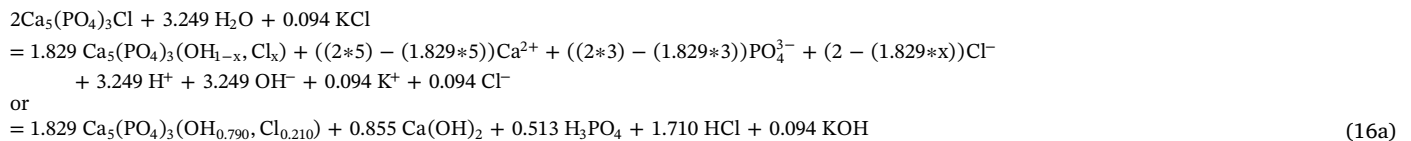
or



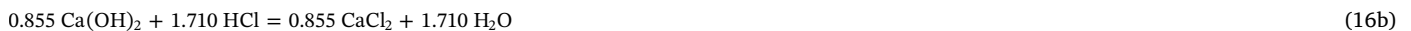
(15)

The dissolution reaction in the system chlorapatite-H<sub>2</sub>O ( $X_{\text{KCl}} = 0.00$ ) is characterized with a very slight excess of HCl in the aqueous solution, however the aqueous solution has a pH value of 7.5 (Table 2b).

chlorapatite-H<sub>2</sub>O ( $X_{\text{KCl}} = 0.20$  and  $\text{pH} = 6.5$ )



The dissolution reaction with  $X_{\text{KCl}} = 0.20$  is initially defined as two precipitating coupled neutralization reactions in which the amount of dissolved  $\text{Ca}(\text{OH})_2$  reacts immediately with  $\text{HCl}$  to form  $\text{CaCl}_2$  and  $\text{H}_2\text{O}$  (Eq. (16b)) and the amount of  $\text{KOH}$  reacts completely with  $\text{H}_3\text{PO}_4$  to form  $\text{K}_3\text{PO}_4$  and  $\text{H}_2\text{O}$  (Eq. (16c)):



The excess remaining  $\text{H}_3\text{PO}_4$  from the resulting reaction (Eq. (16d)) in the aqueous solution produces the slightly acidic pH of 6.5 (Table 2b):



## References

- Agangi, A., Kamenetsky, V.S., McPhie, J., 2010. The role of fluorine in the concentration and transport of lithophile trace elements in felsic magmas: insights from the Gawler Range Volcanics, South Australia. *Chem. Geol.* 273, 314–325.
- Anderson, G.M., Burnham, C.W., 1967. Reactions of quartz and corundum with aqueous chloride and hydroxide solutions at high temperatures and pressures. *Am. J. Sci.* 265, 12–27.
- Andreoli, M.A.G., Smith, C.B., Watkeys, M., Moore, J.M., Ashwal, L.D., Hart, R.J., 1994. The geology of the Steenkampskraal monazite deposit, South Africa; implications for REE-Th-Cu mineralization in charnockite-granulite terranes. *Econ. Geol.* 89, 994–1016.
- Antignano, A., Manning, C.E., 2008. Fluorapatite solubility in  $\text{H}_2\text{O}$  and  $\text{H}_2\text{O-NaCl}$  at 700 to 900 °C and 0.7 to 2.0 GPa. *Chem. Geol.* 251, 112–119.
- Aranovich, L.Y., Newton, R.C., 1996.  $\text{H}_2\text{O}$  activity in concentrated  $\text{NaCl}$  solutions at high pressures and temperatures measured by the brucite-periclase equilibrium. *Contrib. Mineral. Petrol.* 125, 200–212.
- Aranovich, L.Y., Newton, R.C., 1997.  $\text{H}_2\text{O}$  activity in concentrated  $\text{KCl}$  and  $\text{KCl-NaCl}$  solutions at high temperatures and pressures measured by the brucite-periclase equilibrium. *Contrib. Mineral. Petrol.* 127, 261–271.
- Aranovich, L.Y., Newton, R.C., Manning, C.E., 2013. Brine-assisted anatexis: experimental melting in the system haplogranite- $\text{H}_2\text{O-NaCl-KCl}$  at deep-crustal conditions. *Earth Planet. Sci. Lett.* 374, 111–120.
- Aranovich, L.Y., Makhlof, A.R., Manning, C.E., Newton, R.C., 2014. Dehydration melting and the relationship between granites and granulites. *Precambrian Res.* 253, 26–37.
- Ayers, J.C., Watson, E.B., 1991. The behaviour and influence of fluids in subduction zones - solubility of apatite, monazite, zircon, and rutile in supercritical aqueous fluids with implications for subduction zone geochemistry. *Phil. Trans. R. Soc. A* 335, 365–375.
- Banks, D.A., Green, R., Cliff, R.A., Yardley, B.W.D., 2000. Chlorine isotopes in fluid inclusions: determination of the origins of salinity in magmatic fluids. *Geochim. Cosmochim. Acta* 64, 1785–1789.
- Bernini, D., Wiedenbeck, M., Dolejš, D., Keppler, H., 2013. Partitioning of halogens between mantle minerals and aqueous fluids: implications for the fluid flow regime in subduction zones. *Contrib. Mineral. Petrol.* 165, 117–128.
- Bradley, R.S., 1962. Thermodynamic calculations on phase equilibria involving fused salts; part I, general theory and application to equilibria involving calcium carbonate at high pressure. *Am. J. Sci.* 260, 374–382.
- Brenan, J., 1993. Partitioning of fluorine and chlorine between apatite and aqueous fluids at high pressure and temperature: implications for the F and Cl content of high P-T fluids. *Earth Planet. Sci. Lett.* 17, 251–263.
- Caciagli, N.C., Manning, C.E., 2003. The solubility of calcite in water at 6–16 kbar and 500–800 °C. *Contrib. Mineral. Petrol.* 146, 275–285.
- Chakhmouradian, A.R., Wall, F., 2012. Rare earth elements: minerals, mines, magnets (and more). *Elements* 8, 333–340.
- Fayek, M., Kyser, T.K., 1997. Characterization of multiple fluid-flow events and rare-earth-element mobility associated with formation of unconformity-type uranium deposits in the Athabasca basin, Saskatchewan. *Can. Mineral.* 35, 627–658.
- Franz, L., Romer, R.L., Klemm, R., Schmid, R., Oberhänsli, R., Wagner, T., Shuwen, D., 2001. Eclogite-facies quartz veins within metabasites of the Dabie Shan (eastern China): pressure-temperature-time-deformation path, composition of the fluid phase and fluid flow during exhumation of high-pressure rocks. *Contrib. Mineral. Petrol.* 141, 322–346.
- Glassley, W.E., Korstgård, J.A., Sørensen, K., 2010. K-rich brine and chemical modification of the crust during continent-continent collision, Nagssugtoqidian Orogen, West Greenland. *Precambrian Res.* 180, 47–62.
- Hansen, E.C., Harlov, D.E., 2007. Whole-rock, phosphate, and silicate compositional trends across an amphibolite- to granulite-facies transition, Tamil Nadu, India. *J. Petrol.* 48, 1641–1680.
- Hansen, E.C., Harlov, D.E., 2009. Orthophosphate and biotite chemistry from orthopyroxene-bearing migmatites from California and South India: the role of a fluid-phase in the evolution of granulite-facies migmatites. *Mineral. Petrol.* 95, 201–217.
- Harlov, D.E., 2012. The potential role of fluids during regional granulite-facies dehydration in the lower crust. *Geosci. Front.* 3, 813–827.
- Harlov, D.E., 2015. Apatite and fluids: a fingerprint for metasomatic processes. *Elements* 11, 171–176.
- Harlov, D.E., Förster, H.-J., 2002. High-grade fluid metasomatism on both a local and a regional scale: the Seward Peninsula, Alaska, and the Val Strona di Omegna, Ivrea-Verbano Zone, Northern Italy. Part I: petrography and silicate mineral chemistry. *J. Petrol.* 43, 769–799.
- Harlov, D.E., Förster, H.J., 2003. Fluid-induced nucleation of (Y + REE)-phosphate minerals within apatite: nature and experiment. Part II. Fluorapatite. *Am. Mineral.* 88, 1209–1229.
- Harlov, D.E., Andersson, U.B., Förster, H.-J., Nyström, J.O., Dulski, P., Broman, C., 2002. Apatite-monzite relations in the Kiirunavaara magnetite-apatite ore, northern Sweden. *Chem. Geol.* 191, 47–72.
- Harlov, D.E., Wirth, R., Förster, H.J., 2005. An experimental study of dissolution-reprecipitation in fluorapatite: fluid infiltration and the formation of monazite. *Contrib. Mineral. Petrol.* 150, 268–286.
- Harlov, D.E., Johansson, L., Van den Kerkhof, A., Förster, H.-J., 2006. The role of advective fluid flow and diffusion during localized, solid-state dehydration: Söndrum Stenhuggeriet, Halmstad, SW Sweden. *J. Petrol.* 47, 3–33.
- Harlov, D.E., Meighan, C.J., Kerr, I.D., Samson, I.M., 2016. Mineralogy, chemistry, and fluid-aided evolution of the pea ridge Fe oxide-(Y + REE) deposit, Southeast Missouri, USA. *Econ. Geol.* 111, 1963–1984.
- Hughes, J.M., Rakovan, J.F., 2015. Structurally robust, chemically diverse: apatite and apatite supergroup minerals. *Elements* 11, 165–170.
- Izraeli, E.S., Harris, J.W., Navon, O., 2001. Brine inclusions in diamonds: a new upper mantle fluid. *Earth Planet. Sci. Lett.* 187, 323–332.
- John, T., Scambelluri, M., Frische, M., Barnes, J.D., Bach, W., 2011. Dehydration of subducting serpentinite: implications for halogen mobility in subduction zones and the deep halogen cycle. *Earth Planet. Sci. Lett.* 308, 65–76.
- Johnson, E.R., Wallace, P.J., Granados, H.D., Manea, V.C., Kent, A.J.R., Bindeman, I.N., Donegan, C.S., 2009. Subduction related volatile recycling and magma generation beneath Central Mexico: insights from melt inclusions, oxygen isotopes and geodynamic models. *J. Petrol.* 50, 1729–1764.
- Jonsson, E., Harlov, D.E., Majka, J., Högdahl, K., Persson-Nilsson, K., 2016. Fluorapatite-monzite-allanite relations in the Grängesberg apatite-iron oxide ore district, Bergslagen, Sweden. *Am. Mineral.* 101, 1769–1782.
- Kusebauch, C., John, T., Barnes, J.D., Klügel, A., Austrheim, H.O., 2015a. Halogen element and stable chlorine isotope fractionation caused by fluid-rock interaction (Bamble Sector, SE Norway). *J. Petrol.* 56, 299–324.
- Kusebauch, C., John, T., Whitehouse, M.J., Klemme, S., Putnis, A., 2015b. Distribution of halogens between fluid and apatite during fluid-mediated replacement processes. *Geochim. Cosmochim. Acta* 170, 225–246.
- Manning, C.E., Aranovich, L.Y., 2014. Brines at high pressure and temperature: thermodynamic, petrologic and geochemical effects. *Precambrian Res.* 253, 6–16.
- Markl, G., Piazzolo, S., 1998. Halogen-bearing minerals in syenites and high-grade marbles of Dronning Maud Land, Antarctica: monitors of fluid compositional changes during late-magmatic fluid-rock interaction processes. *Contrib. Mineral. Petrol.* 132, 246–268.
- Markl, G., Ferry, J.M., Bucher, K., 1998. Formation of saline brines and salt in the lower crust by hydration reactions in partially retrogressed granulites from the Lofoten Islands, Norway. *Am. J. Sci.* 298, 705–757.
- Mortimer, C.E., Beck, J., Müller, U., 2015. Chemie: Das Basiswissen der Chemie, 12. Auflage. Thieme Verlag (712 Seiten) ISBN-10: 3134843129, ISBN-13: 978-3134843125.
- Newton, R.C., Manning, C.E., 2002. Experimental determination of calcite solubility in  $\text{H}_2\text{O-NaCl}$  solutions at deep crust/upper mantle pressures and temperatures: implications for metasomatic processes in shear zones. *Am. Mineral.* 87, 1401–1409.
- Newton, R.C., Manning, C.E., 2005. Solubility of anhydrite,  $\text{CaSO}_4$ , in  $\text{NaCl-H}_2\text{O}$  solutions at high pressures and temperatures: applications to fluid-rock interaction. *J. Petrol.* 46, 701–716.
- Newton, R.C., Manning, C.E., 2006. Solubilities of corundum, wollastonite and quartz in

- H<sub>2</sub>O–NaCl solutions at 800 °C and 10 kbar: interaction of simple minerals with brines at high pressure and temperature. *Geochim. Cosmochim. Acta* 70, 5571–5582.
- Newton, R.C., Manning, C.E., 2010. Role of saline fluids in deep-crustal and upper-mantle metasomatism: insights from experimental studies. *Geofluids* 10, 58–72.
- Newton, R.C., Aranovich, L.Y., Hansen, E.C., Vandenheuve, B.A., 1998. Hypersaline fluids in Precambrian deep-crustal metamorphism. *Precambrian Res.* 91, 41–63.
- Nijland, T.G., Jansen, J.B.H., Majjer, C., 1993. Halogen geochemistry of fluid during amphibolite-granulite metamorphism as indicated by apatite and hydrous silicates in basic rocks from the Bamble Sector, South Norway. *Lithos* 30, 167–189.
- O'Reilly, S.Y., Griffin, W.L., 2000. Apatite in the mantle: implications for metasomatic processes and high heat production in Phanerozoic mantle. *Lithos* 53, 217–232.
- Pan, Y., Fleet, M.E., 1996. Rare earth element mobility during prograde granulite facies metamorphism: significance of fluorine. *Contrib. Mineral. Petrol.* 123, 251–262.
- Patino Douce, A.E., Roden, M., 2006. Apatite as a probe of halogen and water fugacities in the terrestrial planets. *Geochim. Cosmochim. Acta* 70, 3173–3196.
- Petrucci, R.H., Harwood, W.S., Herring, G.E., Madura, J., 2006. *General Chemistry: Principles and Modern Application*, 9th edition. Prentice Hall (1300 pp.).
- Philippot, P., Selverstone, J., 1991. Trace-element-rich brines in eclogitic veins: implications for fluid composition and transport during subduction. *Contrib. Mineral. Petrol.* 106, 417–430.
- Piccoli, P.M., Candela, P.A., 2002. Apatite in igneous systems. *Rev. Mineral. Geochem.* 48, 255–292.
- Pollard, P.J., Pichavant, M., Charoy, B., 1987. Contrasting evolution of fluorine- and boron-rich tin systems. *Mineral. Deposita* 22, 315–321.
- Pourtier, E., Devidal, J.L., Gibert, F., 2010. Solubility measurements of synthetic neodymium monazite as a function of temperature at 2 kbars, and aqueous neodymium speciation in equilibrium with monazite. *Geochim. Cosmochim. Acta* 74, 1872–1891.
- Rapp, J.F., Klemme, S., Butler, I.B., Harley, S.L., 2010. Extremely high solubility of rutile in chloride and fluoride-bearing metamorphic fluids: an experimental investigation. *Geology* 38, 323–326.
- Salvi, S., Fontan, F., Monchoux, P., 2000. Hydrothermal mobilization of high field strength elements in alkaline igneous systems: evidence from the Tamazeght Complex (Morocco). *Econ. Geol.* 95, 559–576.
- Schettler, G., Gottschalk, M., Harlov, D.E., 2011. A new semi-micro wet chemical method for apatite analysis and its application to the crystal chemistry of fluorapatite-chlorapatite solid solutions. *Am. Mineral.* 96, 138–152.
- Schmidt, C., Rickers, K., Bilderback, D.H., Huang, R., 2007. In situ synchrotron radiation XRF study of REE phosphate dissolution in aqueous fluids to 800 °C. *Lithos* 95, 87–102.
- Selverstone, J., Franz, G., Thomas, S., Getty, S., 1992. Fluid variability in 2 GPa eclogites as an indicator of fluid behavior during subduction. *Contrib. Mineral. Petrol.* 112, 341–357.
- Shmulovich, K.I., Yardley, B.W.D., Graham, C.M., 2006. Solubility of quartz in crustal fluids: experiments and general equations for salt solutions and H<sub>2</sub>O–CO<sub>2</sub> mixtures at 400–800 °C and 0.1–0.9 GPa. *Geofluids* 7, 1–17.
- Spear, F.S., Pyle, J.M., 2002. Apatite, monazite, and xenotime in metamorphic rocks. *Rev. Mineral. Geochem.* 48, 293–335.
- Taghipour, S., Kananian, A., Harlov, D., Oberhänsli, R., 2015. Kiruna-type iron oxide-apatite deposits, Bafq District, Central Iran: fluid-aided genesis of fluorapatite-monazite-xenotime assemblages. *Can. Mineral.* 53, 479–496.
- Touret, J.L.R., 2001. Fluids in metamorphic rocks. *Lithos* 55, 1–25.
- Tropper, P., Manning, C.E., 2005. Very low solubility of rutile in H<sub>2</sub>O at high pressure and temperature, and its implications for Ti mobility in subduction zones. *Am. Mineral.* 90, 502–505.
- Tropper, P., Manning, C.E., 2007a. The solubility of fluorite in H<sub>2</sub>O and H<sub>2</sub>O–NaCl at high pressure and temperature. *Chem. Geol.* 242, 299–306.
- Tropper, P., Manning, C.E., 2007b. The solubility of corundum in H<sub>2</sub>O at high pressure and temperature and its implications for Al mobility in the deep crust and upper mantle. *Chem. Geol.* 240, 54–60.
- Tropper, P., Manning, C.E., 2011. Solubility of CePO<sub>4</sub> monazite and YPO<sub>4</sub> xenotime in H<sub>2</sub>O and H<sub>2</sub>O–NaCl at 800 °C and 1 GPa: implications for REE and Y transport during high-grade metamorphism. *Chem. Geol.* 282, 58–66.
- Wannamaker, P.E., Caldwell, T.G., Doerner, W.M., Jiracek, G.R., 2004. Fault zone fluids and seismicity in compressional and extensional environment inferred from electrical conductivity: the New Zealand Southern Alps and U.S. Great Basin. *Earth Planets Space* 56, 1171–1176.
- Webster, J.D., Kinzler, R.J., Mathez, E.A., 1999. Chloride and water solubility in basalt and andesite melts and implications for magmatic degassing. *Geochim. Cosmochim. Acta* 63, 729–738.
- Williams-Jones, A.E., Migdisov, A.A., Samson, I.M., 2012. Hydrothermal mobilization of the rare earth elements – a tale of “ceria” and “yttria”. *Elements* 8, 355–360.
- Yardley, B.W.D., 1985. Apatite composition and the fugacities of HF and HCl in metamorphic fluids. *Mineral. Mag.* 49, 77–79.
- Yardley, B.W.D., Graham, J.T., 2002. The origins of salinity in metamorphic fluids. *Geofluids* 2, 249–256.
- Young, E.J., Myers, A.T., Munson, E.L., Conklin, N.M., 1969. Mineralogy and geochemistry of fluorapatite from Cerro de Mercado, Durango, Mexico. *US Geol. Surv. Prof. Pap.* 650-D, 84–93.
- Zhou, L., Mavrogenes, J., Spandler, C., Heping, L., 2016. A synthetic fluid inclusion study of the solubility of monazite-(La) and xenotime-(Y) in H<sub>2</sub>O–Na–K–Cl–F–CO<sub>2</sub> fluids at 800 °C and 0.5 GPa. *Chem. Geol.* 442, 121–129.